

Modeled and observed atmospheric radiation balance during the West African dry season: Role of mineral dust, biomass burning aerosol, and surface albedo

S. F. Milton,¹ G. Greed,¹ M. E. Brooks,¹ J. Haywood,¹ B. Johnson,¹ R. P. Allan,² A. Slingo,² and W. M. F. Grey³

Received 20 December 2007; revised 21 February 2008; accepted 18 March 2008; published 15 July 2008.

[1] The global radiation balance of the atmosphere is still poorly observed, particularly at the surface. We investigate the observed radiation balance at (1) the surface using the ARM Mobile Facility in Niamey, Niger, and (2) the top of the atmosphere (TOA) over West Africa using data from the Geostationary Earth Radiation Budget (GERB) instrument on board Meteosat-8. Observed radiative fluxes are compared with predictions from the global numerical weather prediction (NWP) version of the Met Office Unified Model (MetUM). The evaluation points to major shortcomings in the NWP model's radiative fluxes during the dry season (December 2005 to April 2006) arising from (1) a lack of absorbing aerosol in the model (mineral dust and biomass burning aerosol) and (2) a poor specification of the surface albedo. A case study of the major Saharan dust outbreak of 6–12 March 2006 is used to evaluate a parameterization of mineral dust for use in the NWP models. The model shows good predictability of the large-scale flow out to 4–5 days with the dust parameterization providing reasonable dust uplift, spatial distribution, and temporal evolution for this strongly forced dust event. The direct radiative impact of the dust reduces net downward shortwave (SW) flux at the surface (TOA) by a maximum of 200 W m^{-2} (150 W m^{-2}), with a SW heating of the atmospheric column. The impacts of dust on terrestrial radiation are smaller. Comparisons of TOA (surface) radiation balance with GERB (ARM) show the “dusty” forecasts reduce biases in the radiative fluxes and improve surface temperatures and vertical thermodynamic structure.

Citation: Milton, S. F., G. Greed, M. E. Brooks, J. Haywood, B. Johnson, R. P. Allan, A. Slingo, and W. M. F. Grey (2008), Modeled and observed atmospheric radiation balance during the West African dry season: Role of mineral dust, biomass burning aerosol, and surface albedo, *J. Geophys. Res.*, 113, D00C02, doi:10.1029/2007JD009741.

1. Introduction

[2] Considerable uncertainties still exist in our knowledge and modeling of the radiative and energy balance of the Earth/atmosphere system. Aerosols influence the radiative balance of the earth by scattering and absorbing solar radiation and absorbing and reemitting terrestrial radiation (the direct effect), but also by modifying the physical properties and lifetime of clouds by acting as cloud condensation nuclei (indirect effect) [Haywood and Boucher, 2000]. While fully prognostic aerosols are now included in many state-of-the-art climate models [e.g., Bellouin *et al.*, 2007] the computational cost has meant that operational numerical weather prediction (NWP) models have largely

relied on annual or seasonally varying climatologies to model the radiative effect of aerosols [Tarré *et al.*, 1984; Tegen *et al.*, 1997; Cusack *et al.*, 1998]. However, there has been growing evidence of the need for predictive capability for aerosols (and in particular mineral dust) in NWP models, both to improve the modeled atmospheric radiative balance [Haywood *et al.*, 2005; Perez *et al.*, 2000; Grini *et al.*, 2006; Heinold *et al.*, 2007] but also to provide predictions of air quality and aerosol production, transport and deposition for humanitarian, commercial and military purposes [Barnum *et al.*, 2004; Liu *et al.*, 2007]. A number of dust/aerosol short-range prediction systems are operational. These include (1) versions of the Dust Regional Atmospheric Model (DREAM) system based on the NCEP Eta model [Nickovic *et al.*, 2001] run by groups at the Barcelona Supercomputing Center (<http://www.bsc.es/projects/earthscience/DREAM>) and Tel Aviv University (<http://wind.tau.ac.il/dust8/dust.html>) and (2) the U.S. Navy's Navy Aerosol Analysis and Prediction System (NAAPS) global (<http://www.nrlmry.navy.mil/aerosol>) and COAMPS regional [Liu *et al.*, 2007] systems. An intercomparison of eight dust models (including some of those above) in the Dust Model Intercomparison

¹Met Office, Exeter, UK.

²Environmental Systems Science Centre, University of Reading, Reading, UK.

³Department of Geography, Swansea University, Swansea, UK.

Project (DMIP) over Asia study [Uno *et al.*, 2006] highlighted some of the major uncertainties associated with numerical predictions of mineral dust. From the Met Office perspective we are interested in the prediction of dust in NWP forecasts to (1) provide short-range dust predictions to military customers, (2) evaluate the dust parameterizations against detailed in situ and research aircraft observations for specific dust events, (3) investigate the impacts of dust on the weather and general circulation in forecasts from weekly to seasonal timescales, and (4) provide evaluation of the dust parameterization on weather timescales, to help inform its development for climate prediction (similar to the strategy advocated by Phillips *et al.* [2004]).

[3] Observations of the global and regional atmospheric radiative energy balance are still limited. The radiation balance at the surface is not well observed globally compared to the top of the atmosphere (TOA), which has been observed from satellites for a number of years [Barkstrom *et al.*, 1989; Wielicki *et al.*, 1996]. Measurements of the surface radiation balance are available from dedicated sites, although these are almost exclusively over land [Wild, 1999; Wild *et al.*, 2006]. The most comprehensive measurements are from the permanent sites operated by the US Department of Energy Atmospheric Radiation Measurement (ARM) program [Ackerman and Stokes, 2003]. During 2006 measurements of the radiation (and surface energy) balance have been available over West Africa in conjunction with the African Monsoon Multidisciplinary Analysis (AMMA) international project, with networks of surface flux (and sonde stations) aimed at understanding the West African monsoon system [Redelsperger *et al.*, 2006]. At Niamey, Niger (13.51°N, 2.11°E) the ARM Mobile Facility (hereinafter ARM-MF) made detailed measurements of the surface and atmospheric profile with a wide range of active and passive instruments. This deployment of the ARM-MF was as part of the Radiative Atmospheric Divergence Using ARM Mobile Facility, GERB Data, and AMMA Stations (RADAGAST) project [Miller and Slingo, 2007]. GERB has been providing high spatial (50 km) and temporal (approximately 15 min) resolution observations of the TOA radiation balance over Africa, Europe and surrounding oceans since 2003 [Harries *et al.*, 2005]. Broadband radiative fluxes from the GERB instrument have already proven useful in identifying systematic deficiencies in the radiative properties of clouds, aerosols and surface properties in the global NWP version of the Met Office Unified Model (MetUM) [Allan *et al.*, 2005, 2007]. The lack of mineral dust in NWP has been identified as a major determinant of systematic error growth in the outgoing longwave radiation (OLR) over the Sahara [Haywood *et al.*, 2005]. During 2006, the AMMA special observing periods (SOPs) also made use of several research aircraft, in situ and satellite observations to understand different aspects of the West African Monsoon system. The Met Office were closely involved in the Dust and Biomass-burning Experiment (DABEX), and the Dust Outflow and Deposition to the Ocean (DODO 1 and 2) using the Met Office/NERC FAAM BAe 146 aircraft, with the NWP models predicting for the West African region (see papers in this volume).

[4] In terms of modeling for Africa the Met Office has a global NWP model (40 km grid) and a regional African model (20 km grid) running operationally. A Saharan Crisis

Area Mesoscale Model (CAMM) with 17 km grid spacing and including a parametrization of mineral dust [Woodward, 2001], has been run in research mode during the DABEX and DODO SOPs [Greed *et al.*, 2008].

[5] The aim of this paper is to evaluate the radiation balance at the TOA and surface in the Met Office global operational NWP model against the observational data from the ARM-MF in Niamey and GERB broadband radiative fluxes. The dry season is chosen in order to focus on the role of mineral dust and biomass burning aerosols in the radiative balance of the atmosphere. Section 2 provides details of the model, dust parametrization and surface and satellite observations. Section 3 provides summary measures of global NWP model performance in terms of radiative fluxes, surface energy balance, and surface meteorology. Section 4 investigates the role that predictions of mineral dust within NWP forecasts have on the radiative flux errors. The continental-scale Saharan dust event of 6–12 March 2006 [Slingo *et al.*, 2006] is used as a case study in this context.

2. Models and Observations

2.1. Global Model Formulation and Data

[6] The global NWP version of MetUM [Cullen, 1993] is run to 6 days ahead, twice a day, from the 0000 UTC and 1200 UTC analyses. The dynamical core is a semi-implicit, semi-Lagrangian, nonhydrostatic formulation [Davies *et al.*, 2005]. The horizontal resolution is 0.5625° longitude by 0.375° latitude (640 × 481 grid points) which equates to 40 km grid spacing in midlatitudes (and 63 km at the equator). Fifty levels are used in the vertical with a model lid at 65 km. A four dimensional data assimilation (4D-Var) system has been used since October 2004 [Rawlins *et al.*, 2007]. The model physical parameterizations are very similar to those used in the Met Office Hadley Centre atmospheric climate model HadGAM1 [Martin *et al.*, 2006]. The two-stream radiation scheme of [Edwards and Slingo, 1996] is used in the global NWP model with a 3 h calling frequency. A simple background aerosol climatology is also included [Cusack *et al.*, 1998]. This takes account explicitly of 5 aerosol species (water soluble, dust, soot, oceanic, and stratospheric sulphates). The next generation climate model includes an improved representation of the emission, transport, and deposition of aerosols [Bellouin *et al.*, 2007]. Data from the short-range (12–36 h) global NWP forecasts have been used for evaluation against observations (section 3). Use of short-range forecasts ensures that errors in the circulation are kept to a minimum, making it easier (though nontrivial) to ascribe errors in the model to deficiencies in existing parameterization schemes or to missing physical processes.

2.2. Dust Parameterization

[7] A parameterization of mineral dust emission, transport, and deposition originally developed for climate applications has been run in the NWP models [Woodward, 2001]. Dust is specified in six size bins spanning 0.06–60 μm. The parameterization includes dust uplift based on Marticorena *et al.* [1997], with dependencies on fractions of clay, silt, and sand, as well as soil moisture, vegetative fraction, a friction velocity threshold (see later discussion) and the

surface layer friction velocity itself. The advection of dust is by a tracer advection scheme. The parameterization also accounts for wet deposition due to precipitation scavenging, and dry deposition from gravitational settling and turbulent mixing. The radiative properties of dust are modeled assuming spherical particles in each bin size with appropriate refractive indices. Mie scattering theory is used to obtain the dust optical properties averaged over six spectral bands in the SW and nine spectral bands in the LW. While the Mie scattering theory calculations assume spherical particles, electron microscope imagery [e.g., *Chou et al.*, 2008] does show a variety of shapes and sizes and a median aspect ratio of 1.7 during the DABEX campaign. Efforts have been made to model Saharan dust particles by mixtures of oblate and prolate spheroids, using sophisticated T-matrix calculations [e.g., *Mishchenko et al.*, 1997]. These calculations reveal significant differences in the back scatter, but differences of less than 10% in total optical cross sections, single scattering albedo and asymmetry factor. Thus the assumption of spherical particles appears reasonable given the host of other uncertainties associated with the modeling efforts.

[8] Initial trials of the dust parameterization in the Saharan CAMM gave unrealistic dust loadings and a number of improvements to the dust scheme implemented in the latest development cycle of the climate model (HadGEM2) were subsequently trialed as detailed below:

[9] 1. The dry threshold friction velocity term is now taken from *Iversen and White* [1982].

[10] 2. Horizontal dust flux calculations have been extended to include sand particles up to 2000 μm . The vertical flux is still assumed to consist of particles between 0.06 and 60 μm .

[11] 3. The size distribution of the vertical flux is assumed to follow parent soil size distribution, rather than the size distribution of the horizontal flux.

[12] 4. Excessive dust production on steep orographic slopes has been inhibited.

[13] Two further changes were implemented in the NWP models. The emission of dust depends critically on the clay, silt, and sand fractions in the soils data set. The $1^\circ \times 1^\circ$ [*Wilson and Henderson-Sellers*, 1985] soils data set was considered too coarse for the NWP application and was replaced by the International Geosphere Biosphere Programme (IGBP) 1 km data set (see *Greed et al.* [2008] for more details). The threshold friction velocity for dust uplift is defined as

$$U_t^* = A \log_{10}(D_{rep}) + BW + C \quad (1)$$

where D_{rep} is a representative particle diameter in each bin, W is the soil moisture in the top (10 cm deep) model layer and A, B , and C are empirical constants. In sensitivity tests in the NWP models a value for C of -0.15 m s^{-1} gave reasonable aerosol optical depths (AODs) in the range 1–4. Modeling the dust uplift remains an area of considerable uncertainty in dust parameterizations [*Uno et al.*, 2006].

2.3. Observations

2.3.1. ARM Mobile Facility in Niamey

[14] As part of the RADAGAST project the U.S. Atmospheric Radiation Measurement (ARM) program [*Ackerman and Stokes*, 2003] stationed the ARM-MF in Niamey, Niger

(13.51°N, 2.11°E) during November 2005 to January 2007. The ARM-MF produces a wide range of atmospheric measurements [*Miller and Slingo*, 2007]. We use surface radiative flux measurements from broadband radiometers to evaluate the shortwave (SW) and longwave (LW) downwelling and upwelling components. Radiative flux measurements are made every minute. The surface sensible and latent heat fluxes from the model are also compared with ARM-MF measurements of the turbulent fluxes made using an eddy correlation measurement technique with data every 30 min. Sonde data are available four times per day (0530, 1030, 1730, and 2230 UTC). The high vertical resolution sonde data are processed onto model height levels for evaluation purposes.

[15] Care must be taken in comparing a 40 km global model grid box with data from a single observation site. The main problem is the grid box represents heterogeneous terrain over that region, but the observation site is representative of the specific local conditions. The ARM-MF was located at Niamey Airport over a bare soil surface [see *Miller and Slingo*, 2007, Figure 5], a second site was located 50 km distant at Banizoumbou, and although more representative of the sparsely vegetated Sahel [*Miller and Slingo*, 2007, Figure 6], it has more basic instrumentation. Where possible, specific errors for the Niamey site are confirmed with measurements over a wider domain (e.g., TOA radiative fluxes and MODIS albedos in following sections). For this study we concentrate on the Niamey site and have used the nearest model grid point for comparison. The land surface characteristics of this grid point consist of predominantly grassland (77%), broad leaf trees (15%) and bare soil (8%). The model 3 hourly averaged fluxes are taken from the 12–36 h range of the 1200 UTC operational forecasts. The ARM data are averaged up from the 1 min time sampling to 3 h averages to match the model fluxes.

2.3.2. GERB and SEVIRI Data

[16] The GERB instrument aboard the Meteosat-8 weather satellite routinely provides broadband SW and LW radiative fluxes from measurements of the total and SW radiances at the top of the atmosphere [*Harries et al.*, 2005]. Calibrated SW radiances are converted to fluxes using angular distribution models (ADM), which are themselves a function of the identified scene type derived from the Spinning Enhanced Visible and Infrared Imager (SEVIRI [*Schmetz et al.*, 2002]) on Meteosat-8. For the LW radiance to flux conversion a simple regression between radiance and flux is used, based on radiative transfer calculations. In addition to GERB we also make use of SEVIRI for identifying the dust plume during the March dust outbreak. Both instruments have a temporal resolution of around 17 min and spatial scales of 50 km for GERB and 3.3 km for SEVIRI. The GERB data has an accuracy of 2.25% for SW irradiance and 0.96% for LW irradiance. The application of ADMs for radiance to flux conversions in the SW can introduce further errors, which may be substantial in episodes of heavy aerosol burdens. This is discussed further in section 4. Further details of the GERB instrument and its use to evaluate the MetUM are given by *Allan et al.* [2005, 2007]. The GERB data used in this study are the edition 1 ARG (Averaged, Rectified, Geolocated) broadband fluxes averaged up to 3 h for comparison with the model.

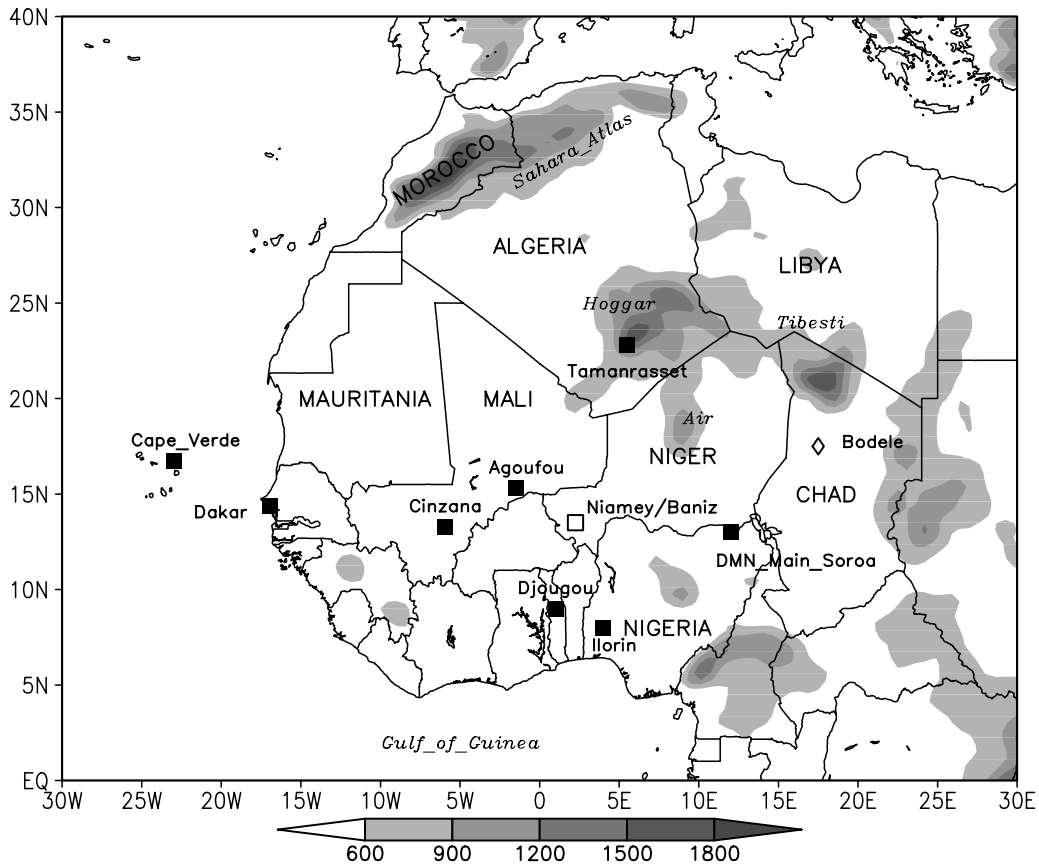


Figure 1. Map of West Africa showing ARM Mobile Facility sites in Niamey/Banizoumbou, Niger (open square), and operational AERONET sites (solid square) used in this study. The diamond marks the position of the Bodélé Depression in Chad, a major source of Saharan dust. The model orography is shown in grey shading with contour interval of 300 m. (Operational global NWP model with approximately 60 km resolution at equator.)

2.3.3. AERONET Data

[17] In order to quantify the aerosol loading we use the aerosol optical depth (AOD) product from the Sun photometer at a variety of AERONET (http://aeronet.gsfc.nasa.gov/new_web/index.html) sites [Holben *et al.*, 1998]. The site at Banizoumbou (Figure 1), 50 km from Niamey, is used to evaluate the model aerosol for the Niamey grid point. This provides AODs at wavelengths 440, 675, 870 and 1020 nm. For all sites the quality controlled and cloud screened level 2 data product is used. The model diagnoses AODs at 380, 440, 550, 670, 870 and 1020 nm.

2.3.4. Ozone Monitoring Instrument Data

[18] Surface based monitoring of aerosols is limited to the coverage provided by the AERONET observations. Satellite remote sensing measurements provide the best opportunity for a global view of aerosol distributions. The Total Ozone Mapping Spectrometer (TOMS) has been providing measurements of absorbing aerosols for over two decades (including NIMBUS-7 1979–1993 and Earth Probe 1996–present), measuring back scattered radiances in the near Ultra Violet (UV) to calculate an Aerosol Index (AI) [Hsu *et al.*, 1999]. The ozone monitoring instrument (OMI) on board the Aura research satellite (2004–present) has continued the TOMS record. We use the OMI AI to provide a qualitative evaluation of the NWP model’s dust evolution

during the March 2006 Saharan dust outbreak. Christopher *et al.* [2008], (this volume) propose a method for deriving more quantitative AOD information on a daily basis over the Sahara using monthly statistical relationships between daily TOMS/OMI AI and the AOD from the narrow swath Multi Angle Imaging Spectroradiometer (MISR), available once every 9 days over Africa. This is used by Greed *et al.* [2008] to evaluate dust in the Met Office Saharan CAMM.

2.3.5. MODIS

[19] The Moderate Resolution Imaging Spectroradiometer (MODIS) albedo products (MCD43C1) from Terra and Aqua platforms are used to evaluate the model surface albedo, and MODIS images of the March dust plume are shown for comparison with the model.

3. Surface and Top of the Atmosphere Energy Balance in the Global NWP Model: December 2005 to April 2006

[20] In this section we consider the dry season atmospheric radiative (and energy) balance of the operational global NWP model, ARM observations at the Niamey site, and GERB observations for the closest pixel to Niamey.

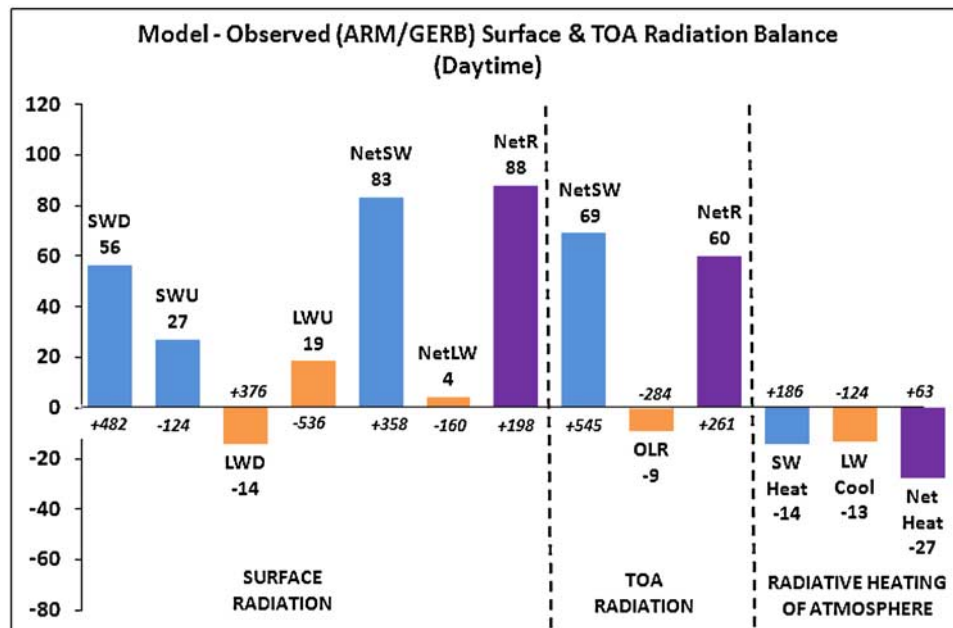


Figure 2. Seasonally averaged daytime (0600–1800 UTC) surface and TOA radiation balance over Niamey (Niger) between 13 January and 16 March 2006. Bars represent the model biases in radiative fluxes measured against surface observations from the ARM Mobile Facility and TOA radiative fluxes from GERB. The observed fluxes are shown along the zero axis (next to bars). Downward fluxes are defined as positive. Units $W m^{-2}$.

3.1. Seasonal Mean Radiative Balance and Divergence

[21] The seasonal mean radiative and surface energy balance for 13 January to 16 March 2006 are shown in Figure 2. Fluxes are defined as positive downward and a positive error (model – observation) implies too much downward flux at the surface or TOA. We concentrate on daytime fluxes (0600–1800 UTC), with discussion of the full diurnal cycle in section 3.3.

[22] The errors in the modeled daytime surface radiation balance at Niamey are dominated by the shortwave (SW) fluxes (Figure 2). The model overestimates the surface downward SW flux by $+56 W m^{-2}$ (12%). Others have discussed similar features in GCMs [e.g., Wild, 1999] citing possible reasons for underestimates as (1) lack of coarse mode aerosol forcing in the models, (2) lack of cloud cover, (3) an underestimate of SW cloud forcing due to poorly defined cloud optical properties, (4) an underestimate of the water vapor in the column, or (5) radiative errors in model’s definition of water vapor absorption. Given the low water loadings during the dry season in both model and observations (1–3 cm column water vapor), it is unlikely that errors in column water vapor are responsible for the large differences in downward SW radiation between the model and ARM data. The possible error sources are further explored in section 3.4. The upward or reflected surface SW is underestimated by $+27 W m^{-2}$ (22%), despite the overestimate in downward SW flux, suggesting problems with our modeled surface albedo. These two SW errors combine positively to give an overestimate of $+83 W m^{-2}$ (23%) in the net downward SW at the surface. The error in the net longwave (LW) radiative flux at the surface is negligible, at only $+4 W m^{-2}$ (2.5%) underestimate. This is partly due to canceling errors in the upward and downward LW compo-

ments. The downward LW shows a $-14 W m^{-2}$ (4%) underestimate, consistent with either (1) too cool or too dry a model atmosphere, (2) lack of aerosol, or (3) lack of cloud forcing. The upward LW is also underestimated by a similar amount, $+19 W m^{-2}$ (4%).

[23] At the TOA the net downward SW is overestimated by $+69 W m^{-2}$ (13%), giving an underestimate in the planetary albedo due to either (1) too small a surface albedo, (2) lack of scattering from aerosols, or (3) an underestimate in cloud SW radiative forcing or a lack of cloud cover. The outgoing LW radiation (OLR) is in better agreement with the GERB observations, with a small overestimate of $-9 W m^{-2}$ (3%).

[24] As the principal aim of the RADAGAST project is to characterize the radiative divergence across the atmosphere, we have carried out a simple calculation using the daytime radiative fluxes outlined above. For the observations (ARM, GERB) the SW heating of the atmosphere is $+186 W m^{-2}$ and the LW cooling $-124 W m^{-2}$, with a net radiative heating $+63 W m^{-2}$ (Figure 2). For the model the SW heating of the atmosphere is underestimated by $-14 W m^{-2}$ (8%) and the LW cooling is overestimated by a similar amount, $-13 W m^{-2}$ (10%). The final error in the net radiative heating of the model column is $-27 W m^{-2}$, which represents an underestimate of 43% compared to the observed value. Of course, the spatial scales of the global model (60 km at equator), ARM-MF (single point measurement), and GERB (50 km) are all different and care must be taken to properly account for surface heterogeneity. Research is underway within the RADAGAST project to address these scale issues. The aim is to provide a consistent observed surface radiative balance product at the GERB

scale, allowing more accurate estimates of the observed radiative flux divergence [Settle *et al.*, 2007].

[25] If we consider the radiative energy balance averaged over both day and night the SW errors still dominate (not shown). The SW heating is underestimated by 8% and the LW cooling overestimated by 3%. The observed daily mean net radiative cooling of the atmosphere is -62 W m^{-2} compared to -74 W m^{-2} for the model. This equates to an error in the net radiative cooling of the atmosphere of around -0.1 K/d . This increased radiative cooling has implications for the hydrological cycle, with the model atmosphere being more unstable.

3.2. Subseasonal Variability in Surface Radiative Fluxes

[26] Scatterplots of model versus ARM surface radiative fluxes for 4 December 2005 to 13 April 2006 are shown to investigate the variability in the model errors across the season (Figure 3). The downward SW flux is consistently biased toward too high values. Errors are of the order $+50 \text{ W m}^{-2}$ on average, and in excess of $+300 \text{ W m}^{-2}$ on some occasions, most notably for the 8 March dust event (shown by the green squares). The upward SW flux shows the opposite error, with the model underestimating the reflected SW in virtually all cases. The seasonally averaged surface albedo (SWup/SWdown) is estimated as 18% for the model and 26% for the ARM observations. This suggests either the model surface is not reflective enough or the observed in situ surface properties (bare soil) are not representative of the wider area covered by the model grid box, which includes both bare soil and vegetation. However, independent aircraft observations of surface albedo, measured in DABEX using Eppley pyranometers during low-level 500ft runs between Niamey and Banizoumbou (roughly the size of 1 model grid box), give a mean surface reflectance of around 28%. The likelihood then is that the model grid box mean albedo is in error (see section 3.4). It is interesting that the 8 March dust event shows small errors in the upward SW. This is because the downward SW is grossly overestimated in the model on this day because of a lack of mineral dust aerosol radiative forcing. This compensates for the discrepancy in the surface albedo to give realistic upward SW fluxes. However, the net downward SW radiation still shows large errors on 8 March. Overall the errors in downward and upward SW radiation combine positively, as noted earlier, to give a large systematic overestimate in net downward SW radiation at the surface (Figure 3e).

[27] The longwave (LW) broadband surface fluxes show less systematic bias in the scatterplots (Figures 3b, 3d, and 3f). This was also seen in the seasonal averages. For downward LW, the largest errors (approximately -60 W m^{-2}) are again for the 8 March dust event, suggesting that some of the underestimate in the model may be a failure to capture the enhanced greenhouse effect associated with mineral dust [Haywood *et al.*, 2005]. The upward LW flux shows errors more strongly linked to the diurnal cycle. At night the upward LW is systematically too large by $20\text{--}30 \text{ W m}^{-2}$. During the early part of the day the model underestimates the upward LW, whereas in late afternoon and early evening the model shows an overestimate (see also Figure 4). Part of this error can be explained by the use of a 3 h radiation time

step. The LW increments calculated at the beginning of a radiation time step are persisted for the following 3 h. This introduces an approximate 1.5 h lag in the modeled LW fluxes compared to the 3 h mean made up from the 1 min sampled ARM observations. The model clear-sky SW fluxes do not suffer from this effect as they are calculated using the average solar zenith angle over the 3 h period. Both cloudy SW and LW fluxes persist the radiative effect of the cloud diagnosed from the beginning of the radiation time step. This can introduce large radiative flux errors in situations where the cloud field is evolving rapidly (see Walters *et al.* [2006] for more details). The afternoon overestimate is also consistent with too much downward SW radiation and too much heating of the surface. The systematic nature of the SW errors and more random scatter of the LW errors are evident in the net fluxes (Figures 3e and 3f). Although the LW fluxes do reveal a more systematic error behavior with respect to the evolution of the diurnal cycle.

3.3. Diurnal Cycle in Surface and TOA Energy Balance

[28] The mean diurnal cycle in the surface and TOA radiative balance and the surface energy balance components (net radiation, sensible and latent heating) are shown in Figure 4. The ground heat flux measurements are not available from the ARM site so it is not possible to fully close the surface energy balance.

[29] At TOA the model net SW radiative flux is overestimated by around 100 W m^{-2} compared to GERB, while the errors in the OLR are much smaller, with largest discrepancies in late afternoon and at night (Figure 4a). At the surface we see the errors already noted comprising an overestimate in downward SW and underestimate in upward (reflected) SW (Figure 4b). For the terrestrial radiation the downward LW has largest errors during the day when the flux is underestimated. The upward LW clearly shows the time lag introduced by the 3 h radiation time step.

[30] For the daytime surface energy balance during the dry season, net radiation at the surface is largely balanced by the sensible heat flux, with latent heat fluxes negligible ($5\text{--}10 \text{ W m}^{-2}$) (Figure 4c). The model overestimate in net downward radiation (approximately $+150 \text{ W m}^{-2}$) is largely balanced by a similar overestimate in the sensible heat flux. At night the net radiative cooling is too large in the model and so is the (downward) sensible heat flux in the stable boundary layer. This latter error is well understood as being due to the use of “long-tailed” stability functions for mixing in stable conditions. Although giving poor agreement with in situ flux measurements and Monin-Obukhov theory, this enhanced mixing in stable conditions seems to be required by global scale NWP (and climate) models to prevent excessive cooling of the deep continental interiors in winter (see Beljaars [2001] for discussion of this issue). In the global NWP version of the MetUM “short-tailed” stability functions have recently been implemented over the sea, only retaining the long-tailed stability functions over land [Brown *et al.*, 2008].

[31] Finally, the impact of these errors in surface energy balance can clearly be seen in the 1.5 m temperatures of the model compared to ARM-MF (Figure 4d). Daytime temperatures are systematically too large up to a maximum of

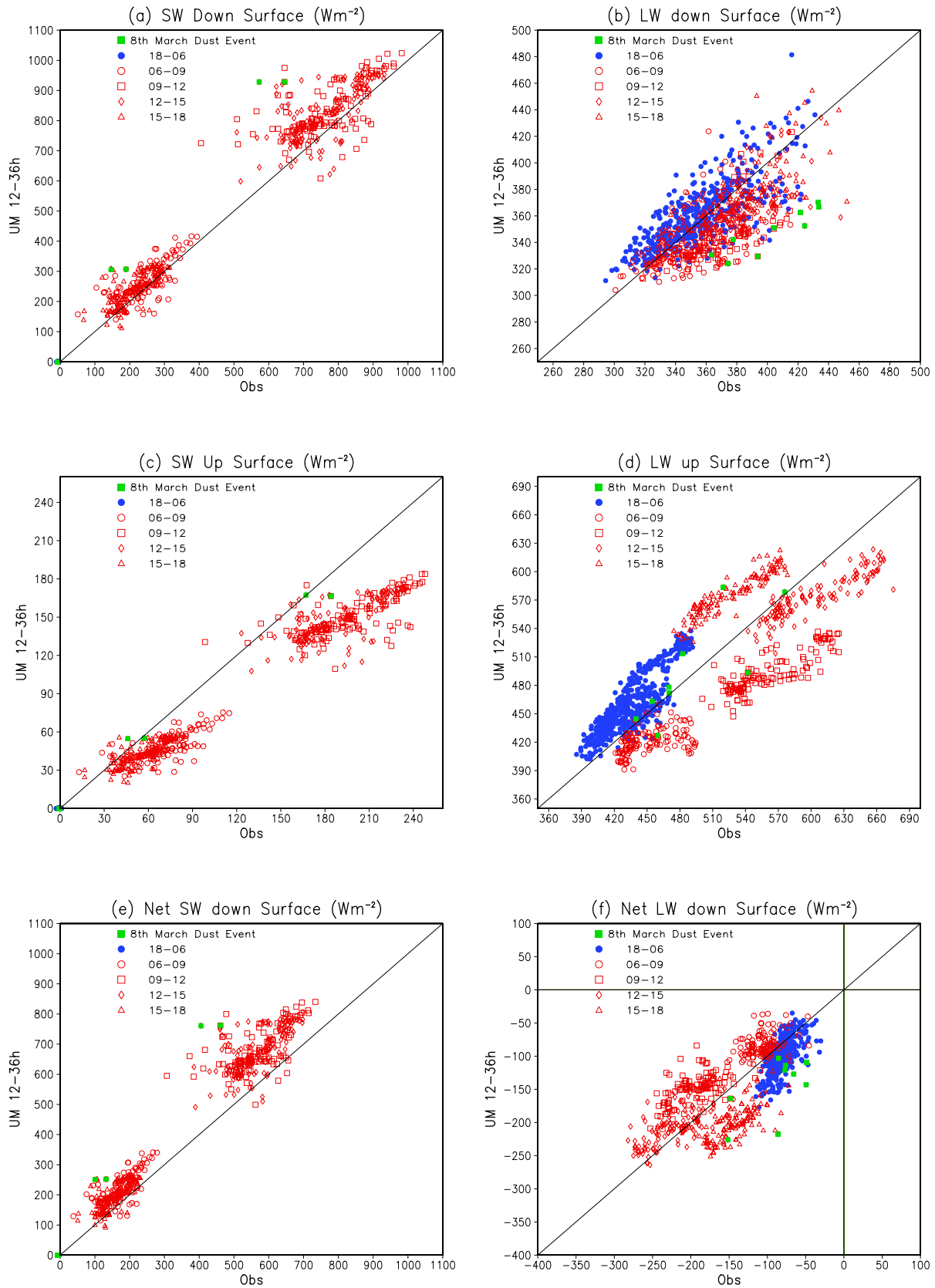


Figure 3. Scatterplots of surface radiative fluxes from MetUM 12–36 h forecast (initialized from 1200 UTC analysis) versus ARM observations at the ARM Mobile Facility in Niamey showing (a) downward SW, (b) downward LW, (c) upward SW, (d) upward LW, (e) net SW, and (f) net LW. Three hourly fluxes are shown from model and observations for the dry season period 4 December 2005 to 13 April 2006. Units W m^{-2} .

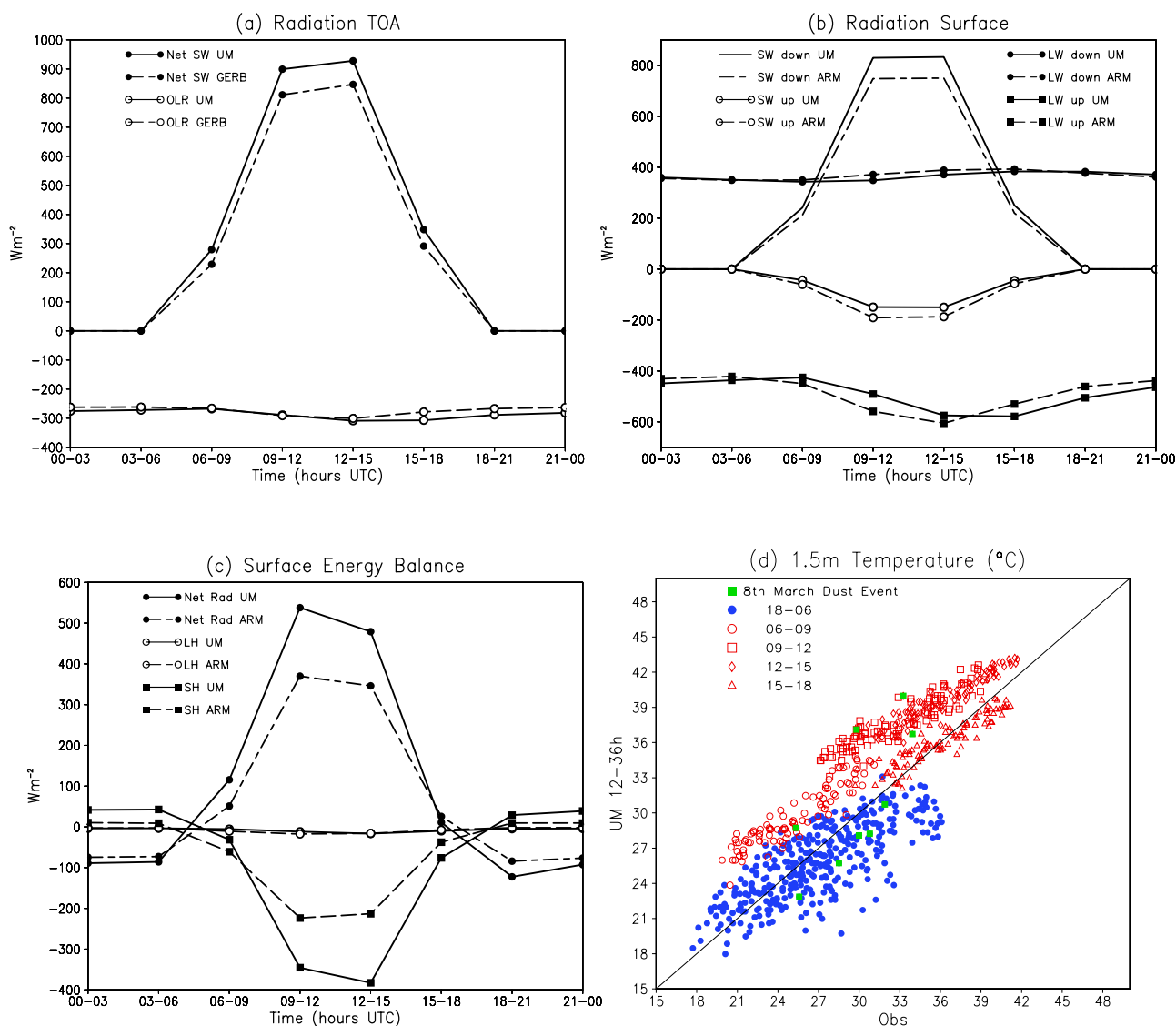


Figure 4. Diurnal cycle of (a) TOA radiation balance, (b) surface radiation balance, and (c) surface energy balance components. The MetUM 12–36 h forecasts are shown against the ARM Mobile Facility observations and the GERB observations for the Niamey pixel. The 3 hourly fluxes are shown for the dry season period 13 January 2006 to 16 March 2006. Units are W m^{-2} . Also shown is (d) scatterplot of model 12–36 h forecasts versus ARM 1.5 m temperatures (every 3 h) for the period 4 December 2005 to 13 April 2006.

+6°C. This is consistent with excessive downward SW heating of the surface and enhanced sensible heating of the near surface layers. At night the model temperature errors are more evenly spread between too warm and too cold.

3.4. Role of Aerosols and Surface Albedo in Shortwave Radiative Balance

[32] The errors in the SW radiative balance are consistent with a failure to model absorbing mineral dust and biomass burning aerosols. We would expect the aerosols to (1) absorb SW radiation, increasing atmospheric warming and reducing downward SW at the surface and (2) scatter SW radiation, again reducing the surface SW flux while increasing the reflected SW flux at TOA (currently too low in the model (Figure 4a)). A dust layer will also increase the downward

LW radiative flux at the surface and decrease the TOA OLR. Both SW and LW effects of aerosols would alleviate the current model deficiencies (Figures 2 and 4).

[33] Comparing errors (model – ARM) in 3 hourly downward SW radiative flux at Niamey with the AODs at 440 nm from the Banizoumbou AERONET site, we see a positive correlation between the periods of large aerosol loadings (AODs > 0.5) and the largest positive errors in downward SW radiation (Figure 5). This clearly shows the role the aerosol in the atmosphere has in modulating the surface SW radiative flux. The 8 March severe dust outbreak shows AODs approaching 4 with a slow decay back to 0.5 over several days. The downward SW errors reached a maximum of 350 W m^{-2} when dust loadings were largest and then showed a steady decrease back to errors of 50–

Impact of Aerosol on UM Downward SW error (Niamey–Banizoumbou)

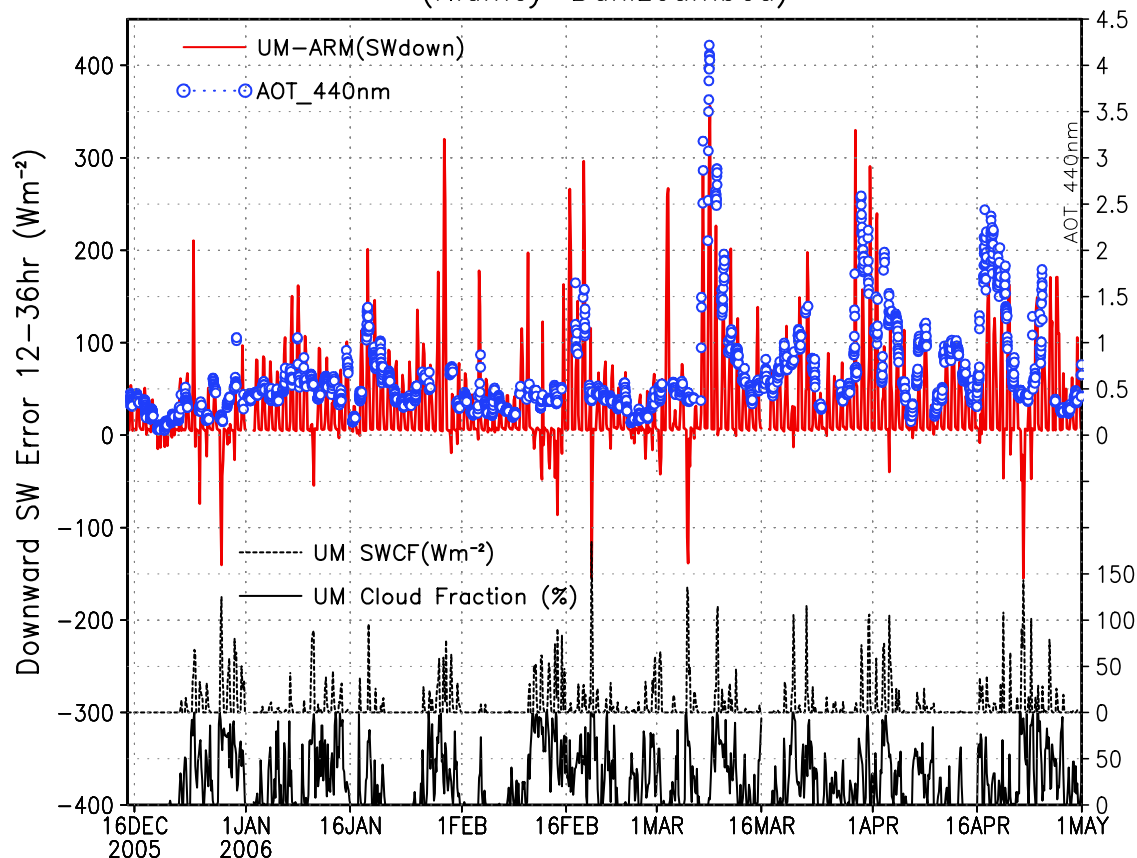


Figure 5. Time series of surface downward shortwave (SW) radiation error (model – ARM-MF) from MetUM 12–36 h forecasts (red line) overlaid with aerosol optical depths (AODs) at 440 nm (circles) from the Banizoumbou AERONET station for 16 December 2005 to 1 May 2006. The downward SW flux error is every 3 h and the AODs every 15 min. The correlation coefficient is 0.5 for the 3 hourly SW flux errors and AOD and 0.59 between the 1200 UTC (midday) SW errors and daily mean AOD. The bottom two traces show the model total cloud fraction (%), solid line) and the model SW cloud forcing (SWCF = cloudy – clear-sky flux) at top of atmosphere (dashed line). These diagnostics give some indication of cloud cover and strength of SWCF in the model through this period (see text for discussion).

100 W m^{-2} as the dust in the atmosphere dispersed. The role of cloud in determining errors in the downward SW radiation cannot be ignored. Figure 5 also shows the modeled total cloud fraction and the model TOA SW cloud forcing (SWCF = cloudy – clear-sky fluxes). Significant amounts of cloud cover are predicted during the season. Most of this is thin high cloud with weak SW cloud forcing ($< 50 \text{ W m}^{-2}$). A number of modeled cloud events have SW cloud forcings $> 100 \text{ W m}^{-2}$ and are associated with negative errors in the downward SW flux, suggesting that the model cloud is thicker or cloud cover more extensive than observed. Allan *et al.* [2007] discuss errors in modeling high cloud detrained from convection in the MetUM. More work is required to define the observed cloud cover from the ARM observations and determine errors in cloud radiative forcing or cloud cover in the model.

[34] To further quantify the role played by the aerosols we have run the E-S radiation code [Edwards and Slingo, 1996] off-line to give an estimate of the downward SW aerosol forcing. The off-line radiative transfer model was initialized

using AOD from the Banizoumbou AERONET site. The aerosol column was assumed to be a mixture of mineral dust and biomass burning aerosol, as found during the Dust and Biomass-burning Experiment (DABEX) (J. Haywood *et al.*, Overview of the Dust and Biomass-burning Experiment and African Multidisciplinary Monsoon Analysis Special Observing Period-0, submitted to *Journal of Geophysical Research*, 2008). The relative proportions of biomass and dust optical depth were estimated from the AERONET Ångström exponent, using an empirical relationship from Johnson *et al.* [2008]. Aerosol optical properties were derived from aircraft observations during DABEX [Johnson *et al.*, 2008; Osborne *et al.*, 2008]. The radiative transfer calculations confirm that most of the error in downward SW in the model can be attributed to aerosol (Figure 6a). As illustrated, it is important to include both aerosol types as the neither dust nor biomass alone can explain the SW errors throughout the time period (Figure 6a). Early in the season at least half the aerosol forcing is from biomass burning aerosol (Figure 6b), whereas later in the season the aerosol

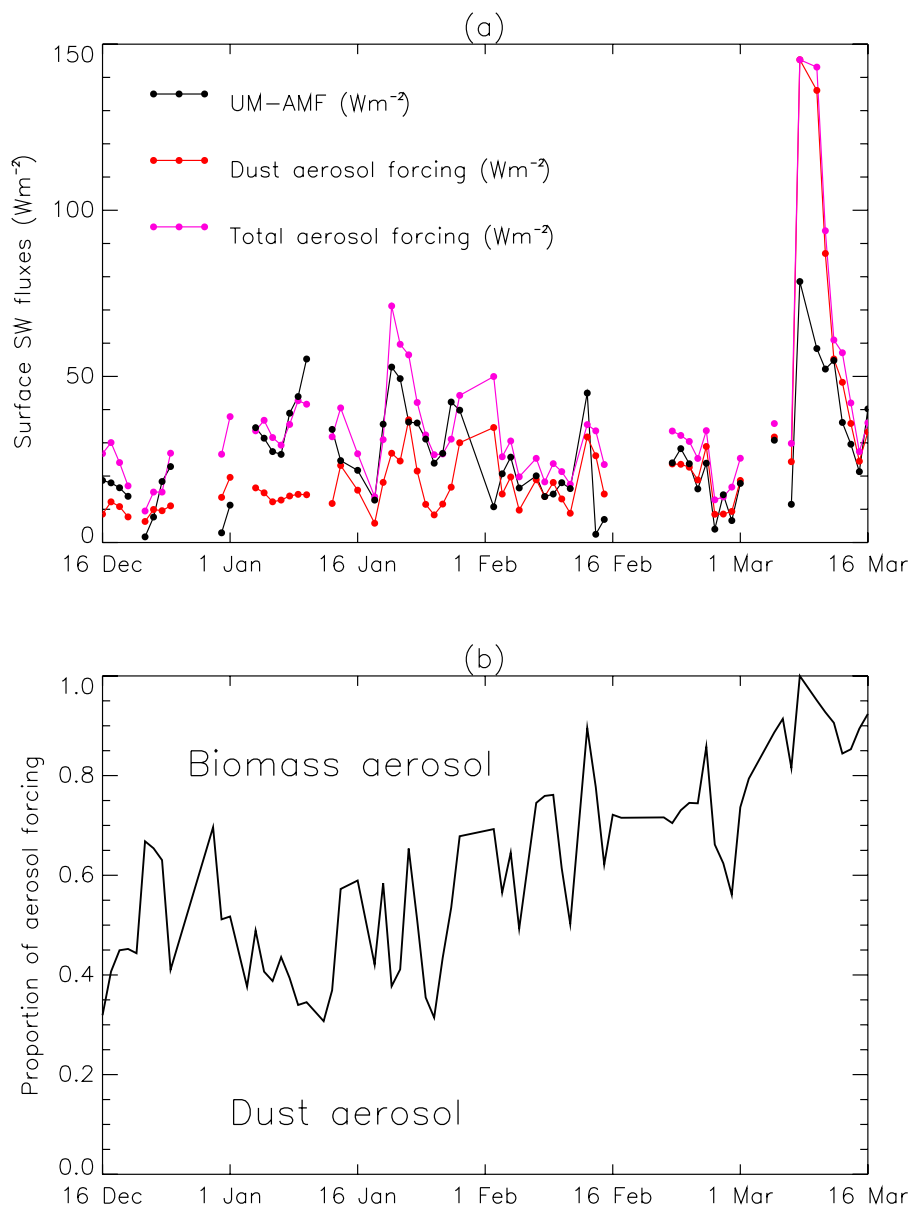


Figure 6. Simulated impact of aerosol SW forcing from off-line E-S radiation scheme forced by aerosol properties from the Banizoumbou AERONET site (16 December 2005 to 16 March 2006). (a) MetUM downward SW error (as in Figure 5) daily averaged and the simulated aerosol SW forcing from the E-S calculations. (b) Fraction of aerosol that is mineral dust estimated from the observed ngstrom exponent at the AERONET site.

forcing is more dominated by mineral dust. Although days with extensive cloud cover in the MetUM or AERONET data have been screened out from this comparison, the remaining discrepancies in downward SW flux are most likely due to discrepancies in modeled versus observed cloud cover not accounted for in the off-line radiative transfer calculations.

[35] The other systematic error at Niamey was an underestimate in the reflected SW flux at the surface, attributed to poorly modeled surface albedo. Prior to May 2007, the global NWP model's surface albedo was specified from the 1° land use data set of *Wilson and Henderson-Sellers* [1985] (hereinafter referred to as WHS85) as a function of soil color state, soil wetness, snow, and vegetation characteristic. As part of the development of the Joint UK Land Environment

Simulator (JULES) land surface scheme, recent research at the University of Swansea Climate and Land Surface Interaction Centre (CLASSIC) has used 6 years of MODIS MCD43C1 Terra/Aqua global albedo product and land cover classification product (MODIS/Terra MOD12C1) to redefine the model bare soil albedo at 0.05° resolution and vegetative albedos for the six plant functional types used in JULES [*Houlieroft et al.*, 2008]. Figure 7 shows comparison of current and revised model albedos with the snow free albedo climatology [*Moody et al.*, 2005] (Figure 7a). With WHS85 albedos the Sahel stands out clearly with an underestimate of up to 15% (Figure 7b), showing that SW errors at Niamey are not solely an issue of grid box versus point observation representativity. Elsewhere, we see the opposite error. Surface albedo is too large over the Sahara,

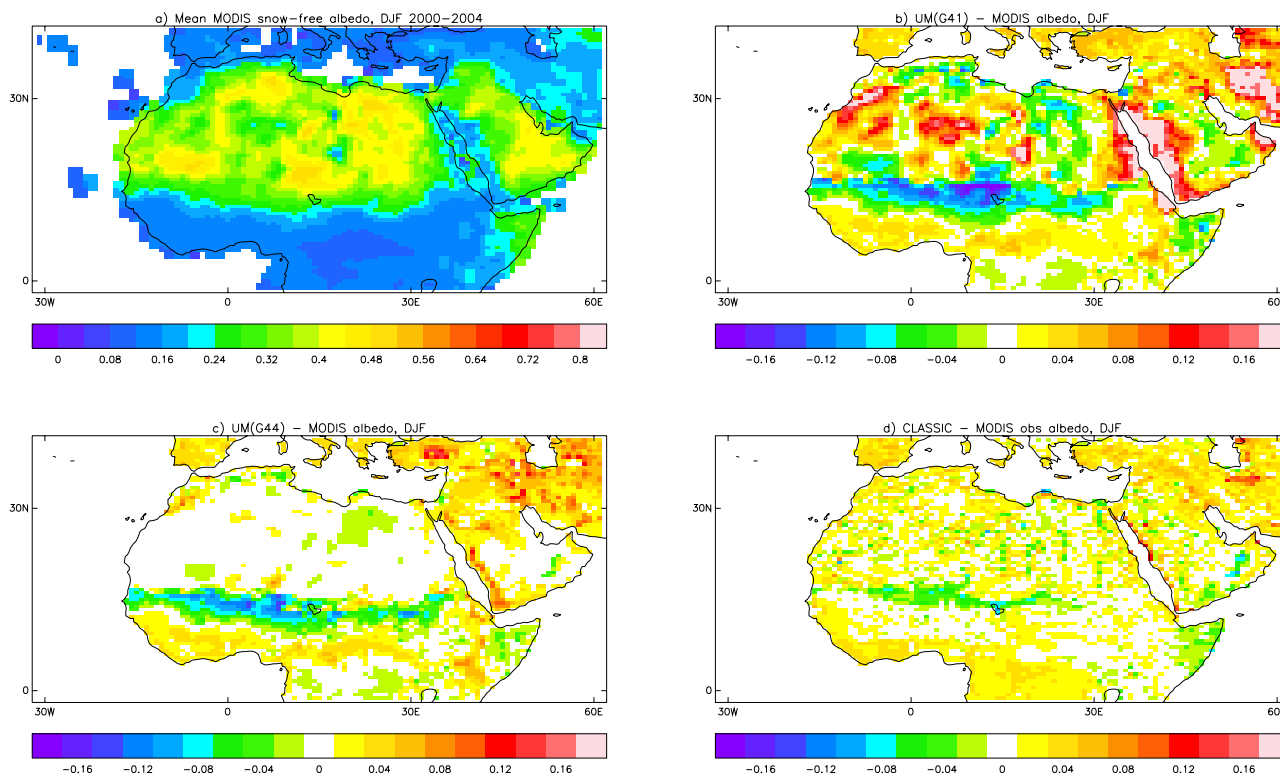


Figure 7. Comparisons of MetUM global NWP model and MODIS surface albedos. (a) Four year average of MODIS annual mean snow-free albedo from *Moody et al.* [2005] and model – MODIS albedo differences for (b) MetUM surface albedos used operationally until 15 May 2007 (model cycle G41), (c) revised MetUM albedos based on MODIS and implemented 15 May 2007 (changes only over sparsely vegetated surfaces, model cycle G44), and (d) further revisions to MetUM albedos for vegetated surfaces and bare soil underlying vegetation to be implemented in 2008.

particularly the orography of the Hoggar, Air and Tibesti (Figure 1), and in the mountainous coastal regions surrounding the Red Sea. Using MODIS data the model bare soil albedos were revised in regions of sparse vegetation for the operational global NWP model (model cycle G44, May 2007). These changes have significantly improved the albedo in the model, correcting many of the biases in the desert regions of the Sahara and Middle East (Figure 7c). Further refinements to the vegetative albedo and to the remaining bare soil albedo under heavily vegetated surfaces have been developed, and are planned for implementation in 2008. These greatly reduce the remaining albedo biases, particularly over the Sahel (Figure 7d). The full impacts of these albedo changes on the weather forecasts and general circulation will be described elsewhere.

[36] Summarizing, during the West African dry season (December–April) the largest errors in the surface and TOA radiation budgets are in the SW radiative fluxes, with too much downward SW radiation at the surface and too little reflected SW at surface and TOA. Comparisons with observations (AERONET, MODIS, GERB) show these errors are consistent with a lack of mineral dust (and biomass burning) aerosol radiative forcing in the model and also to a poor specification of the bare soil and vegetative albedos. These SW errors lead to a daytime warm bias in surface and screen level temperatures. Biases in the OLR and surface LW fluxes are smaller, but may also be consistent with a lack

of mineral dust aerosol. In the next section we investigate how the inclusion of a mineral dust parameterization might help in alleviating some of these radiative flux biases.

4. Dust Outbreak of 6–12 March 2006

4.1. Synoptic-Dynamic Evolution

[37] The observed physical and radiative properties of the major Saharan dust outbreak of 6–12 March 2006 are described by *Slingo et al.* [2006]. Here we look more closely at the evolution of dust and its relation to the large-scale flow as shown by satellite observations and Met Office operational analyses. Figure 8 shows the EUMETSAT RGB dust diagnostic derived from differences amongst three SEVIRI infrared channels (8.7, 10.8, and 12.0 μm). Dust appears as pink and optically thick, high, and cold cloud as dark red. The first frame is for 0000 UTC 6 March 2006 shortly after initiation of the dust storm and shows the dust front located just to the south of the Saharan Atlas mountains (Figure 8a). In the subsequent 12 h the dust front propagates south and west (Figure 8b). A day later, at 1200 UTC 7 March 2006, the dust front encounters the orography of the Hoggar, Air and Tibesti mountains (Figure 1) with clear evidence of intensification of the dust plume as the flow is channeled around the orography and near surface wind speeds are increased (Figure 8c). The dust front reaches Niamey on the morning of 7 March. By 1200 UTC

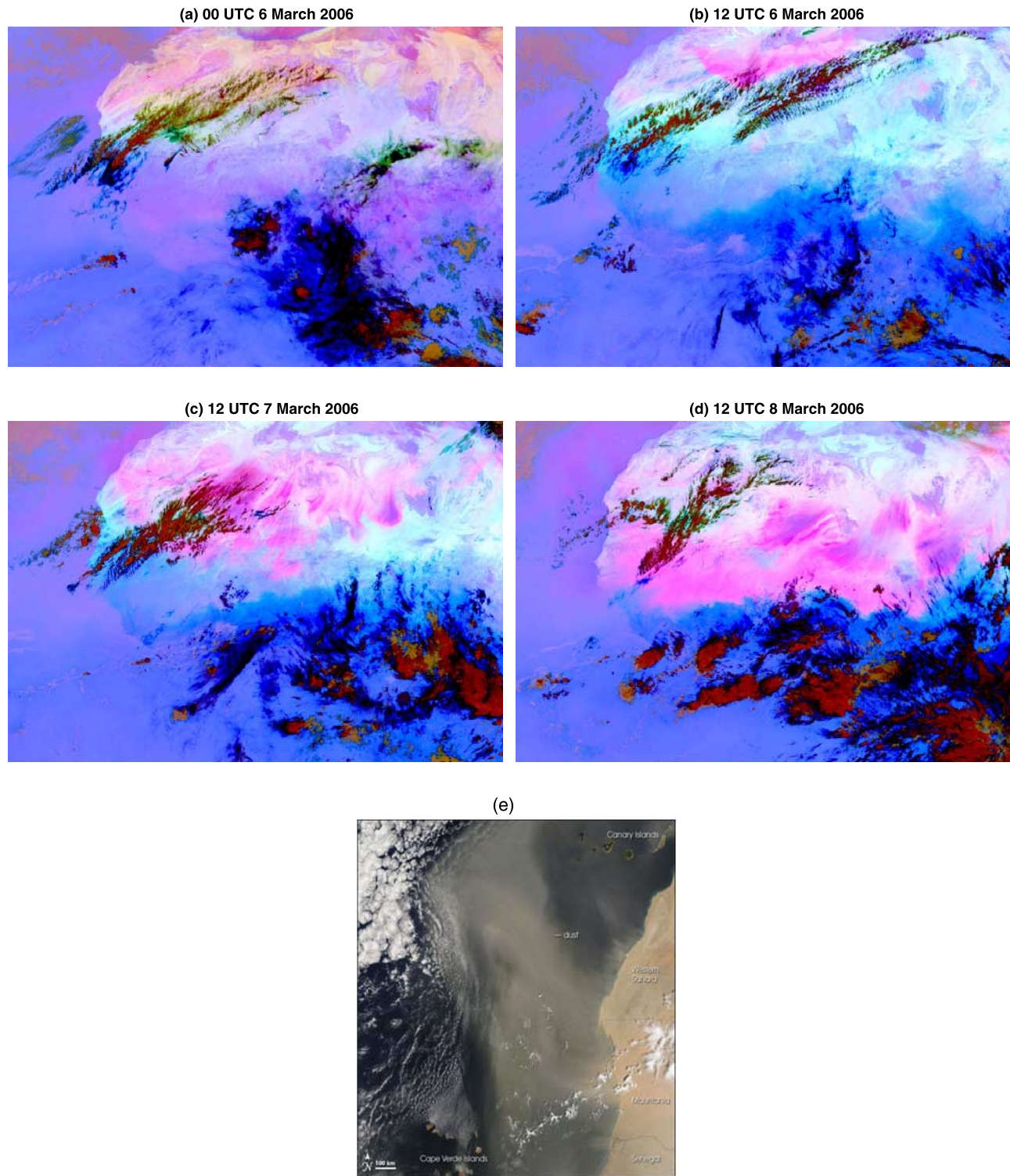


Figure 8. SEVIRI RGB dust product (see text) with dust shown in pink and cold high cloud in dark red. (a) 0000 UTC 6 March, (b) 1200 UTC 6 March, (c) 1200 UTC 7 March, and (d) 1200 UTC 8 March. Also shown is (e) MODIS image for 1200 UTC 8 March 2006.

8 March AODs at Niamey were at their largest values of order 3.5 [*Slingo et al.*, 2006]. Behind the dust front further large emissions of dust occur over preferential sources as the flow is channeled around the Air orography and south of the Tibesti orography over the Bodélé Depression (Figure 8d). A recent study by *Todd et al.* [2008] has

shown that dust emissions over the Bodélé are also strongly driven by diurnal variations in wind speed. This involves the formation of a nighttime low level jet in the stable boundary layer followed by mixing of momentum to the surface after sunrise and subsequent dust uplift. The dust plume propagates out over the tropical Atlantic and the

MODIS imagery shows clearly the bright dust plume over the darker ocean surface at 1200 UTC 8 March (Figure 8e). By 1200 UTC 9 March (not shown) there is a further emission of dust in the east associated with an intensification of near surface winds in this region at this time. A significant amount of dust was also advected eastward over the Mediterranean, with air quality severely degraded in Tel Aviv on 9 March, highlighting the continental scale nature of this dust outbreak.

[38] The synoptic and dynamic evolution bears many similarities to the March 2004 dust event described by *Knippertz and Fink* [2006]. The initiation of the dust storm in the Atlas mountains can be traced back to a tropical-extratropical interaction, involving the building of a large scale ridge in the mid-Atlantic, significant trough extension over southern Europe, and advection of a surface cold front over North Africa. Following *Knippertz and Fink* [2006], the large scale evolution is shown by the Met Office analysis fields of potential vorticity (PV) on the 330 K isentropic surface, midtropospheric vertical velocity field at 6 km, and the streamlines of the model level 1 wind field (10 m) (Figure 9). Between 4 and 5 March the ridge of high pressure in the Atlantic intensifies ahead of a developing low level cyclone/upper level positive PV anomaly upstream near Newfoundland. Over the Mediterranean there is an upper level positive PV anomaly with an area of midtropospheric descending air to its west and ascending air located over the anomaly. In the next 2 days this large-scale upper trough/PV anomaly sweeps eastward, and by 1200 UTC 8 March it is located over the eastern Mediterranean. As this system tracks eastward the region of descending air to its west also tracks slowly eastward across North Africa and intensifies. An anticyclone forms over Morocco and Algeria on 6–8 March on the westward flank of the descending air, and a region of strong surface northerly flow intensifies because of the intense pressure gradients formed between this anticyclone and the cyclone located further east over the Mediterranean. It is this northerly flow that initially lifts the dust in the lee of the Atlas mountains, and propagates dust south and west near the surface in the form of a density current. A vertical north–south section through 0–10°E shows the midtropospheric air at 25°N descending the 310 K isentrope below the large upper tropospheric PV anomaly (Figure 9f). A more detailed investigation of the dynamics is beyond the scope of this paper, but *Knippertz and Fink* [2006] explore the similar March 2004 dust event in considerable detail. They highlight the role of precipitation and evaporational cooling in the dry desert air over the Atlas mountains in intensifying the initial dust front and the role played by the unbalanced dynamics in the anticyclonogenesis over north-west Africa. A similar case of severe Saharan dust outbreak associated with strong southward meridional flow during springtime over the Mediterranean was also discussed by *Özsoy et al.* [2001]. Clearly, other factors such as orographic channeling and diurnal variations in surface wind [*Todd et al.*, 2008] are also important for dust emissions occurring behind the initial dust front.

[39] Some questions we hope to address in the following sections are (1) the degree of predictability associated with this large-scale flow over the Atlantic, Mediterranean, and West Africa; (2) the performance and uncertainties in the

dust generation, transport, and deposition; and (3) the radiative impacts of the parameterized dust compared to observations. A similar regional modeling study using the MesoNH model has been carried out for this Saharan dust outbreak by *Tulet et al.* [2008].

4.2. Modeling the Saharan Dust Outbreak

[40] To illustrate the predictability of the large-scale flow during the dust outbreak we have calculated a series of back trajectories over West Africa from Met Office analyses and forecasts, initialized at 1200 UTC 4 March 2006 (Figure 10). For a target box at 500 m over Niamey on 1200 UTC 8 March 2006, the analyzed back trajectories show the origin of the air in two well defined plumes. One begins over the Atlantic between 6 km and 8 km, while a second originates at low levels in the Gulf of Guinea. The existence of these two distinct plumes points to the convergence zone between the warm moist air from the southwest and the dry desert air from the northeast. The trajectories originating over the Atlantic show a rapid descent over North Africa from 4 km to 500 m, consistent with the area of subsidence discussed in the previous section. The operational global NWP model forecast back trajectories (beginning at day 4 of the forecasts over the target box, 1200 UTC 8 March) show good agreement with the analyses, representing both the midtropospheric air from the north and the low level trajectories from the south. However, the midtropospheric Atlantic trajectories in the forecast originate too far east compared to the analyses. A second set of back trajectories centered on Dakar 1 day later show even better agreement between the forecasts and analyses. In this case the majority of trajectories follow the same path originating in the midtroposphere close to Newfoundland or Iceland, then descending rapidly over North Africa before turning westward over Dakar and into the Atlantic as part of the northeasterly Harmattan flow.

[41] Global model forecasts and sensitivity tests have been carried out to investigate the predictability and direct radiative impact of the dust parameterization in the global NWP model. For reasons of economy these have been carried out at reduced horizontal and vertical resolution (approximately 90 km at equator, and 38 vertical levels) compared to the current operational global NWP forecasts (60 km at equator and 50 vertical levels). The reduced resolution forecast also captures the main features of the event seen in the trajectories and dynamical fields. The following experiments were carried out: (1) NO DUST forecast; (2) DUST Standard, a forecast with standard dust setup as described in section 2.2; and (3) DUST Revised, a sensitivity test to the dust uplift. The parameter C in equation (1) was changed from -0.15 to -0.20 m s^{-1} to promote dust uplift at lower thresholds of the friction velocity.

[42] All forecasts are initialized from a Met Office operational global NWP model analysis for 1200 UTC 4 March 2006, beginning with zero dust loading and spinning up dust during the first few days.

4.2.1. Prediction of the Dust Distribution and Evolution

[43] Figure 11 shows the time evolution of the forecast AODs at 550 nm and the AI from the OMI instrument. At 1200 UTC 6 March 2006 the model shows a dust front stretching from western Algeria to northwest Libya and into

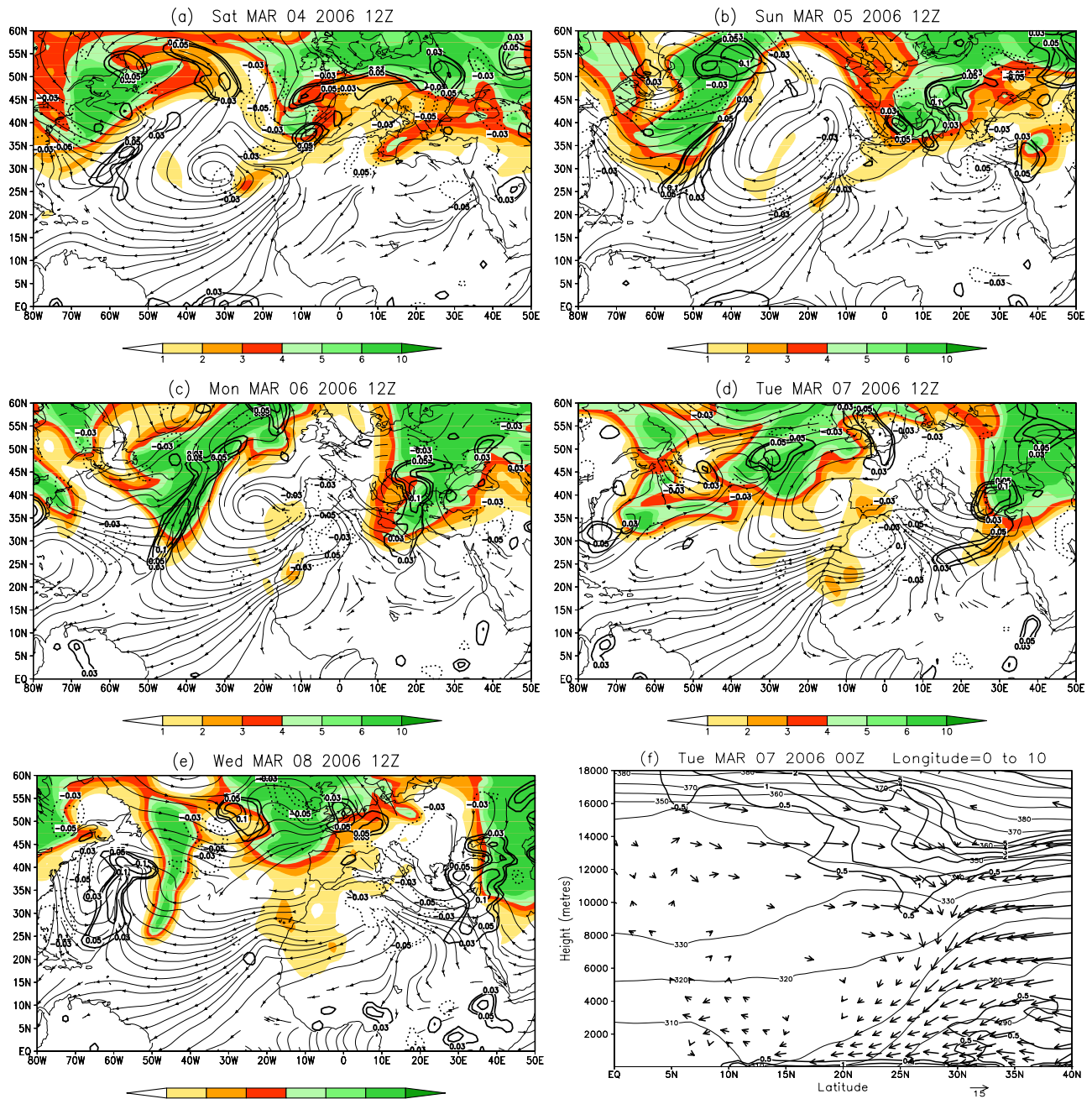


Figure 9. Analyzed PV on 330 K isentropic surface (shaded in PV units of 1), midtropospheric (5.45 km, model level 17) vertical velocity (m s^{-1}) shown as bold contours with ascent ($w > 0$) shown as solid and descent ($w < 0$) shown as dotted, streamlines of the 10 m wind plotted for wind speeds above 3 m s^{-1} . Diagnostics are derived from Met Office operational global NWP analyses. (a–e) Five frames show evolution every 12 h beginning at 1200 UTC 4 March 2006 and ending at 1200 UTC 8 March 2006. (f) Height–latitude cross section averaged over $0\text{--}10^\circ\text{E}$ showing PV (bold contours), potential temperature (thin contours), and the v – w wind field.

the Mediterranean, in good qualitative agreement with the OMI AI. The OMI AI also shows larger amounts of dust over the Bodélé Depression in Chad and over southern Libya. This discrepancy may be due to the model still being in its dust spin-up phase. In the next 24 h the model dust is advected south across a broad front with an intensification of dust concentrations as the low level wind field is channeled and intensified by the topography of the Hoggar,

Air and Tibesti ranges (Figure 1). This is in good agreement with the enhanced dust plumes seen in the SEVIRI dust product (Figure 8). High dust loadings in the OMI data can be seen around Niamey in agreement with the observed passage of the main dust front at the ARM-MF [Slingo *et al.*, 2006]. The model has a weak dust loading with AODs of $0.1\text{--}0.3$ at this time. By 1200 UTC 8 March 2006 both the modeled and observed dust plumes have moved out over

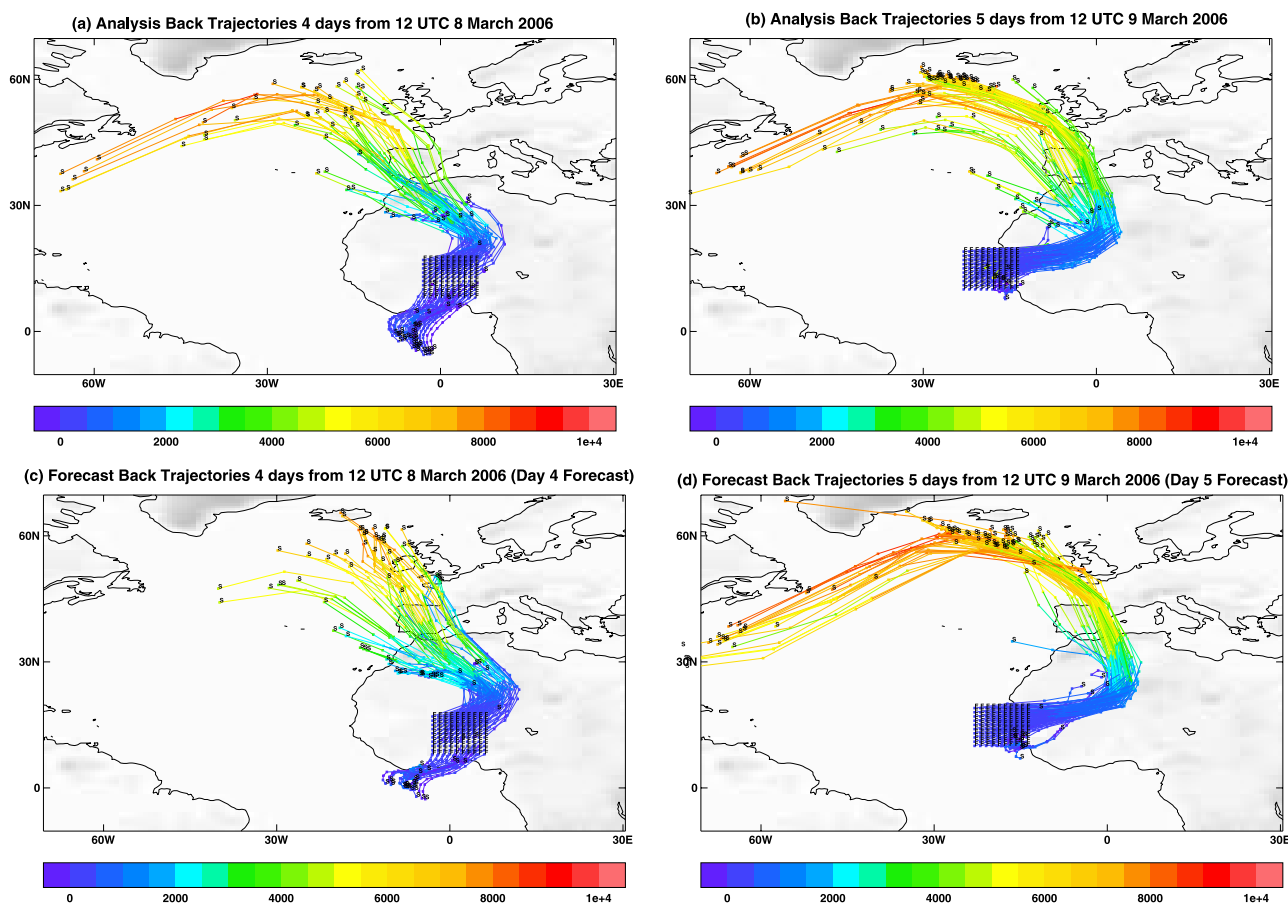


Figure 10. Back trajectories from (a and b) Met Office analyses and (c and d) operational global NWP forecasts. Figure 10a analyzes back trajectories calculated over 4 days (12 h time step) beginning on 1200 UTC 8 March 2006 from a target box at 500 m height centered on Niamey. The end point for the back trajectories is 4 days earlier at 1200 UTC 4 March 2006. Figure 10c is the same as Figure 10a but for forecast back trajectories beginning over the target box on day 4 of the forecast and ending at the analysis time of 1200 UTC 4 March. Figure 10b analyzes back trajectories spanning 5 days beginning over Dakar at 500 m at 1200 UTC 9 March 2006. Figure 10d is the same as Figure 10c but for forecast back trajectories beginning at day 5 of the forecast. The colors represent the height of the trajectories in meters.

the tropical Atlantic and been transported northward over the Canary Islands, while model AODs over Niamey have increased and are close to unity. The exact regions of high dust loading in the model and suggested by the OMI AI show some discrepancies. For example, the model has very high AOD > 4 in the northern Sudan (30°E , 20°N) not observed by OMI, while OMI shows high dust loadings over southern Mali (0°E – 10°W , 10 – 15°N) and directly over the Bodélé Depression where model AODs are small. The Bodélé region is one of the most important sources of dust worldwide [Prospero *et al.*, 2002; Washington *et al.*, 2003]. Although in this case study the global model appears to underestimate dust emissions, a longer series of forecasts from the Saharan CAMM during July 2006 show good qualitative agreement between the model and TOMS AI for this region (not shown).

[44] Further quantitative comparison of the dust evolution can be gained using the AERONET stations (Figure 1) at Banizoumbou, IER Cinzana, Dakar (M’Bour), Cape Verde, Djougou, Agoufou, DMN Maine Soroa and Tamarassat (Figure 12). Overall the model captures the rise in AODs between 7 and 9 March at the various sites but under-

predicts the maximum AODs. At Banizoumbou the AODs reach a maximum of 4 on 8 March whereas the model standard dust parametrization is just greater than 1. The time evolution is well captured with the peak at midday on 8 March and a slow decay of dust thereafter. The model forecast for Cinzana is very similar. A sensitivity test to further reduce the friction velocity threshold for dust uplift by 0.05 m s^{-1} (to a C value of -0.2 m s^{-1} in equation (1)) does increase the maximum modeled AODs to 1.5 at Banizoumbou, but this is still short of the observed values. As noted earlier, the model is capable of achieving higher AODs (e.g., over northern Sudan), so the failure to predict adequate dust at Niamey may be a function of either (1) poorly modeled dust sources, (2) an incorrect soil moisture state, or (3) deficiencies in the modeled near surface wind strength. Todd *et al.* [2008] have shown the importance of vertical resolution and the formulation of the boundary layer parametrization on a model’s ability to capture the diurnal variations in near-surface wind associated with the low level jet over the Bodélé. Work is underway to investigate some of these possibilities (M. Harrison and D. Ackerley, personal communication, 2007). This includes sensitivity to

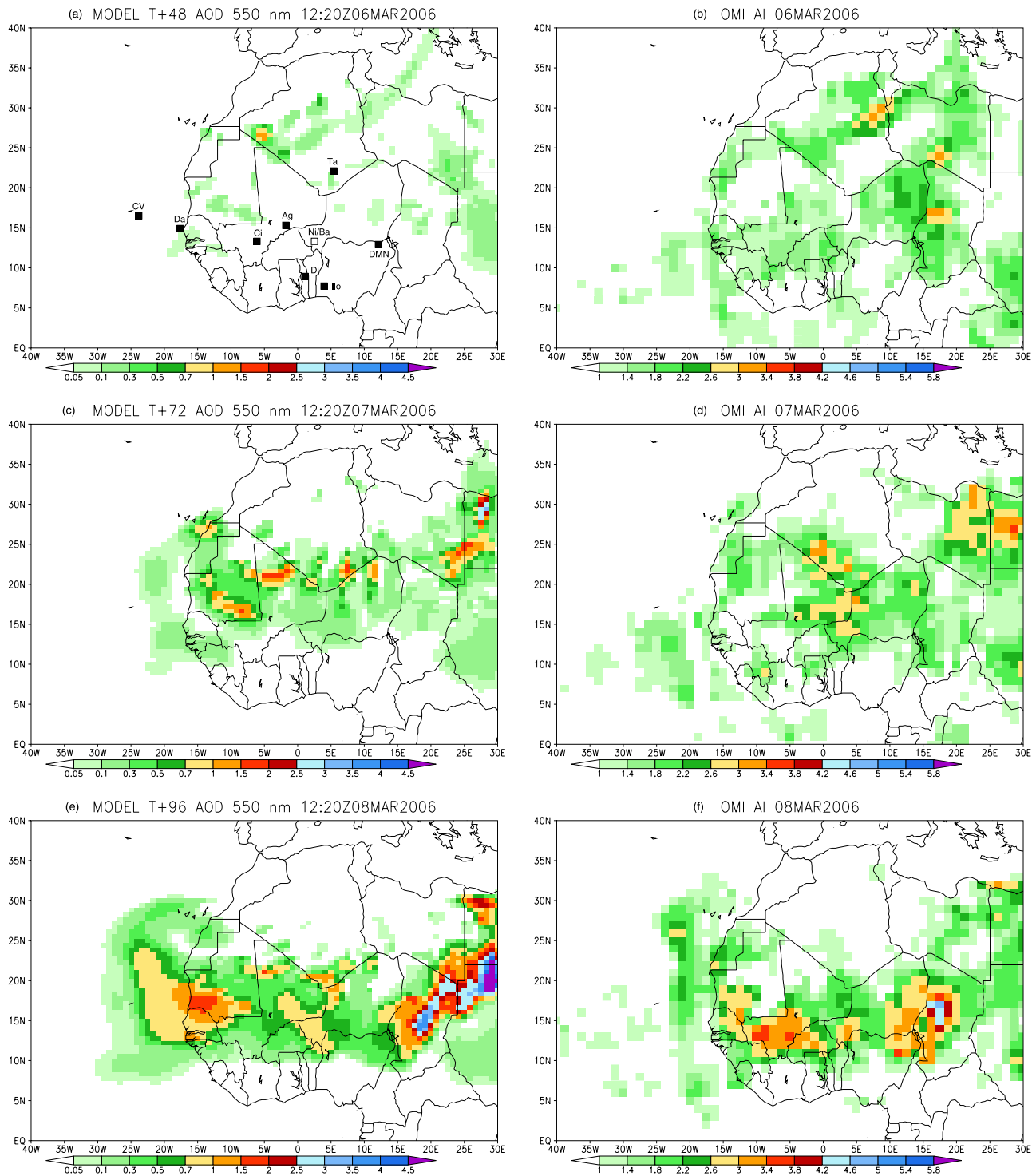


Figure 11. Evolution of dust plume in model and OMI data for (a and b) 6 March, (c and d) 7 March, and (e and f) 8 March 2006. The model AOD is at 550 nm and for the 1200 UTC snapshot, and the OMI AI data are daily means. Note the different scales between model AOD and OMI. The model dust forecasts use the standard dust set up (DUST Standard) and OMI AI. The AERONET stations are shown in Figure 11a.

alternative formulations of dust uplift such as used in the Dust Entrainment and Deposition model (DEAD) scheme [Zender *et al.*, 2003]. Recent work by Grini *et al.* [2005] has tried to build on the observations that preferential source

regions for dust appear to exist [Prospero *et al.*, 2002]. They linked regions of high soil erodibility to those of high surface reflectivity in MODIS data to capture these “preferential” dust source regions. This approach is being trialed

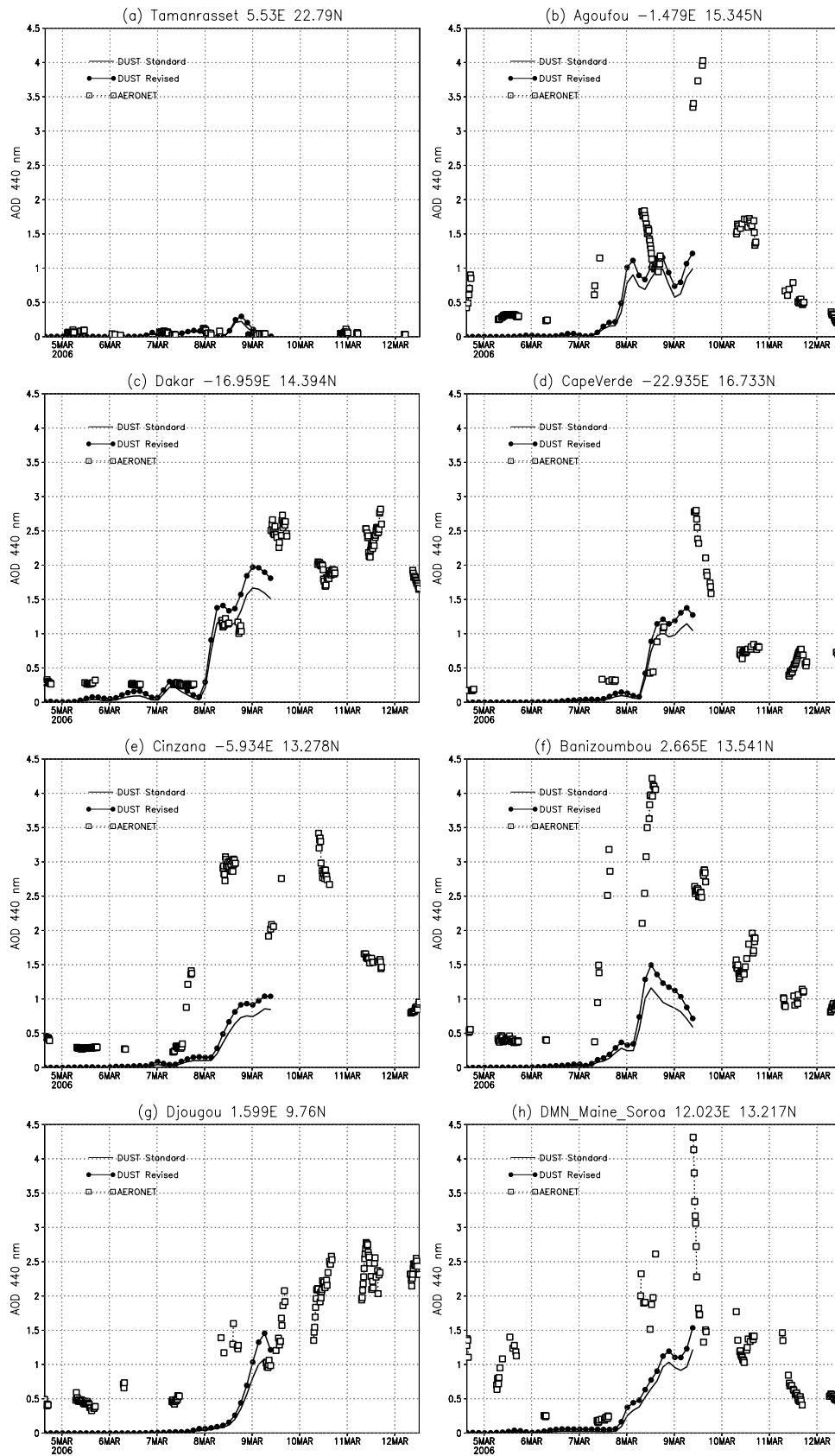


Figure 12. MetUM 5-day forecasts versus AERONET AOD for 1500 UTC 4 March to 1200 UTC 12 March 2006 at (a) Tamanrasset, (b) Agoufou, (c) Dakar, (d) Cape Verde, (e) Cinzana, (f) Banizoumbou, (g) Djougou, and (h) DMN Maine Soroa. These sites are also shown in Figure 1. The model AOD are every 3 h, the AERONET data every 15 min (where data are available).

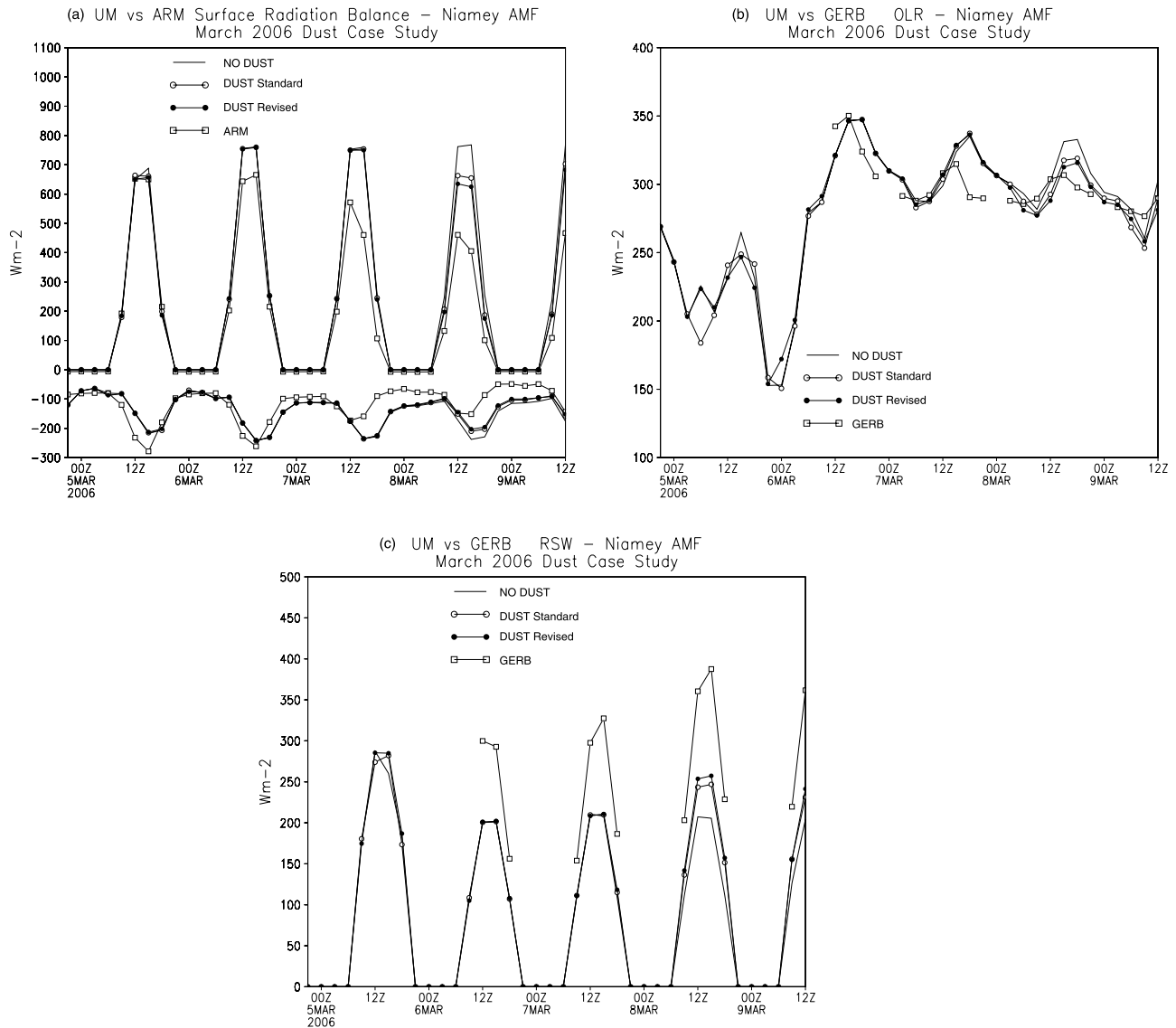


Figure 13. (a) Surface radiative fluxes, MetUM versus ARM-MF observations; (b) OLR TOA, MetUM versus GERB; and (c) MetUM reflected SW at TOA, MetUM versus GERB, during the major Saharan dust outbreak (1800 UTC 5 March to 1200 UTC 9 March 2006). The NO DUST forecast is compared with forecasts using the standard setup (DUST Standard) and the sensitivity to the dust uplift parameters (DUST Revised). Units are W m^{-2} .

in the MetUM. At Dakar the AODs are higher in the model and in better agreement with AERONET observations. This site also shows $\text{AODs} > 2$ out to 12 March in the observations. MODIS and TOMS AOD show this dust plume transported significant dust into the Atlantic between 9 and 18 March reaching as far west as South America. At Cape Verde Islands the initial dust increase on 8 March was well captured by the model (Figure 12d). The observed dust AODs rise to 3 on 9 March but rapidly fall back to values less than 1 as most of the transport into the Atlantic from 9 March onward occurred just south of the Cape Verde Islands. The small dust loadings at Tamanrasset (Figure 12a) throughout this period in both model and observations reflect the high altitude (1377 m) of this site in the Hoggar mountains, with the “dusty” cool density current being

channeled around the highest orography and through the low lying valleys.

4.2.2. Direct Radiative Effect of Mineral Dust: Modeled and Observed

[45] The parametrization of mineral dust takes account of the direct radiative effect on both SW and LW components, with relevant feedbacks on the model’s meteorology. We begin by considering the surface radiative impact of dust in model and ARM observations at the Niamey AMF site at 3 hourly intervals from 2100 UTC 5 March to 1200 UTC 9 March 2006 (Figure 13). The ARM radiative fluxes show net SW of around 650 W m^{-2} on 5 March falling to 550 W m^{-2} on 7 March when dust first arrives at Niamey/Banizoumbou then to 450 W m^{-2} on 8 March when AODs are maximum at Banizoumbou (Figure 12f). *Slingo et al.* [2006] showed that most of the surface downward SW

radiative flux on 8 March comes from the diffuse component due to the high AODs, with the direct radiative flux becoming very small. For the surface net LW there is a decrease from around -300 W m^{-2} to -150 W m^{-2} due to the additional downward LW emission from the dust layer, and also from a cooler atmosphere associated with the advection of colder air over the site from the desert (see skew-T (Figure 16a)). It is difficult to disentangle these two effects in the observations, although we can from the various model runs (see below).

[46] The model net SW is in good agreement with ARM on 5 March. This is due to the presence of cloud over the site (see SEVIRI image for 0000 UTC 6 March (Figure 8a)) which is well captured by the model (see also the low OLR/high reflected SW values in the model at TOA, Figure 13). On 6 March, cloud free conditions and low aerosol loading prevail. The model net SW is too high by 50 W m^{-2} and most of this error can be attributed to the underestimate in surface albedo in the model noted earlier. The modeled AODs are low compared to observations on 7 March (Figure 12), so the radiative impact of the modeled dust is not seen until 8 March. The modeled dust AOD of 1 to 1.5 gives a reduction in net surface SW of around 100 W m^{-2} , which compares with an observed reduction of 200 W m^{-2} between 6 and 8 March for an increase in observed AOD from 0.5 to 4 shown by the AERONET data. A small reduction of 10 W m^{-2} occurs in the modeled net LW on 8 March. The sensitivity test to reduce the threshold friction velocity shows a slightly larger radiative impact (Figure 13) due to the higher AODs predicted (Figure 12f).

[47] At the top of the atmosphere the GERB OLR fluxes at the Niamey pixel show a reduction of around 40 W m^{-2} between 6 and 8 March 2006 (Figure 13b). Reductions in OLR due to the advection of colder air over the site can be seen in the NODUST model forecasts and amount to around 15 W m^{-2} . The radiative impact of dust on OLR in the model is a further reduction of 10 W m^{-2} , giving a total decrease in OLR of 25 W m^{-2} in the model, just over half that observed. The errors (model – GERB) in reflected SW (RSW) at TOA are larger and reflect the combined effect of too low surface albedo and lack of dust in the model forecasts. For the cloud free and low aerosol loading day of 6 March the model RSW is too large by 100 W m^{-2} . A day earlier the model RSW values are significantly larger because of the presence of cloud at Niamey predicted by the model (GERB data is unavailable for this date). During 6–9 March the GERB RSW shows an increase of around 90 W m^{-2} due to the presence of mineral dust. The model forecasts show a smaller radiative impact of $50\text{--}60 \text{ W m}^{-2}$ due to the smaller AODs.

[48] Clearly the prediction of the radiative impact of modeled dust at Niamey is somewhat compromised by the underestimate in AODs. Figure 14 shows the modeled radiative impact (DUST-NODUST) at the surface and TOA for the whole west African domain at 1200 UTC 8 March. The largest impacts are on the net SW fluxes. At the surface there is a reduction in net SW due to the absorption and scattering of solar radiation by the dust layer. Reductions of $>150 \text{ W m}^{-2}$ occur in the tropical Atlantic off Mauritania where modeled AOD > 1 . The TOA net SW (positive downward) shows similar but smaller reductions, with largest effects over the ocean where the

bright dust layer reflects significantly more SW than the dark ocean. The flux divergence (TOA-surface) gives the SW radiative heating on the model atmosphere. The DUST-NODUST difference shows that the dust layer heats the atmosphere in the SW. For terrestrial radiation the net LW surface flux (negative-cooling) is decreased by $10\text{--}40 \text{ W m}^{-2}$ because of the absorption and reemission of LW radiation back to the surface from the dust layer. At TOA the reduction in OLR is somewhat smaller. Consequently, the flux divergence in the LW shows dust cooling the atmosphere by $10\text{--}40 \text{ W m}^{-2}$ (but warming the surface). The net (LW+SW) radiative impact of the dust (not shown) is to warm the atmospheric column, and cool the surface, and overall to provide a negative radiative forcing at the top of the atmosphere.

[49] We can evaluate the modeled TOA radiative balance over other regions of West Africa using the GERB broadband fluxes. Modeled and observed AODs are high for the tropical Atlantic domain off the west coast of Africa ($12\text{--}24^\circ\text{N}$, $18\text{--}23^\circ\text{W}$ (see Figure 11)) and the presence of dust in the model on 8 March brings the reflected SW in much closer agreement to the GERB observations (Figure 15a). However, some care must be taken in interpreting the GERB fluxes during these high dust loadings. The angular dependence models (ADM) used to convert radiances to fluxes currently depend on a scene being identified as clear or cloudy in GERB processing and take no account of dust [Brindley and Russell, 2006]. The presence of high dust loadings may be incorrectly interpreted as cloud and weak dust loadings as clear sky. The use of the cloudy ADM in the presence of dust underestimates GERB fluxes compared to a radiance to flux conversion that tries to take account of dust. The use of the clear-sky ADM means GERB fluxes will be overestimated, with the magnitude of this latter effect varying between 0 and 55 W m^{-2} and 12 W m^{-2} on average (H. Brindley, personal communication, 2007). Although this means the absolute values of the GERB fluxes may be questionable the increased RSW in the model due to dust may still be interpreted as an overall improvement, as the DUST-NODUST changes are probably larger than the GERB uncertainties. For this same Atlantic region the model SW radiative effect efficiency, $\partial F_{\uparrow SW} / \partial AOD_{440}$, can be estimated by plotting the DUST-NODUST change in TOA RSW against the modeled AOD on a point by point basis (Figure 15b). This shows a SW radiative effect efficiency of $+60 \text{ W m}^{-2}$ per unit AOD, in good agreement with observational [Hsu et al., 2000] and previous modeling estimates in this region [Weaver et al., 2002].

4.2.3. Impact of Mineral Dust on Forecast Temperatures

[50] Finally, we consider the impact of mineral dust on the thermodynamic structure and screen level temperatures. The skew-T plot from the ARM-MF sondes at 1730 UTC shows the dramatic change from a deep (3.5 km) dry adiabatic layer on the 6th to a cooler (drier) layer between the surface and 2 km on the 8th, associated with the passage of the cold front (density current) and dust plume (Figure 16a). Comparing the biases (model - sonde) on 8 March at Niamey we can see that the NODUST model shows a warm bias of 2.5°C in the lowest 2 km. The inclusion of dust in the model reduces this bias by 1°C (Figure 16b). The dust layer also gives a small warming between 2 and 3.5 km due

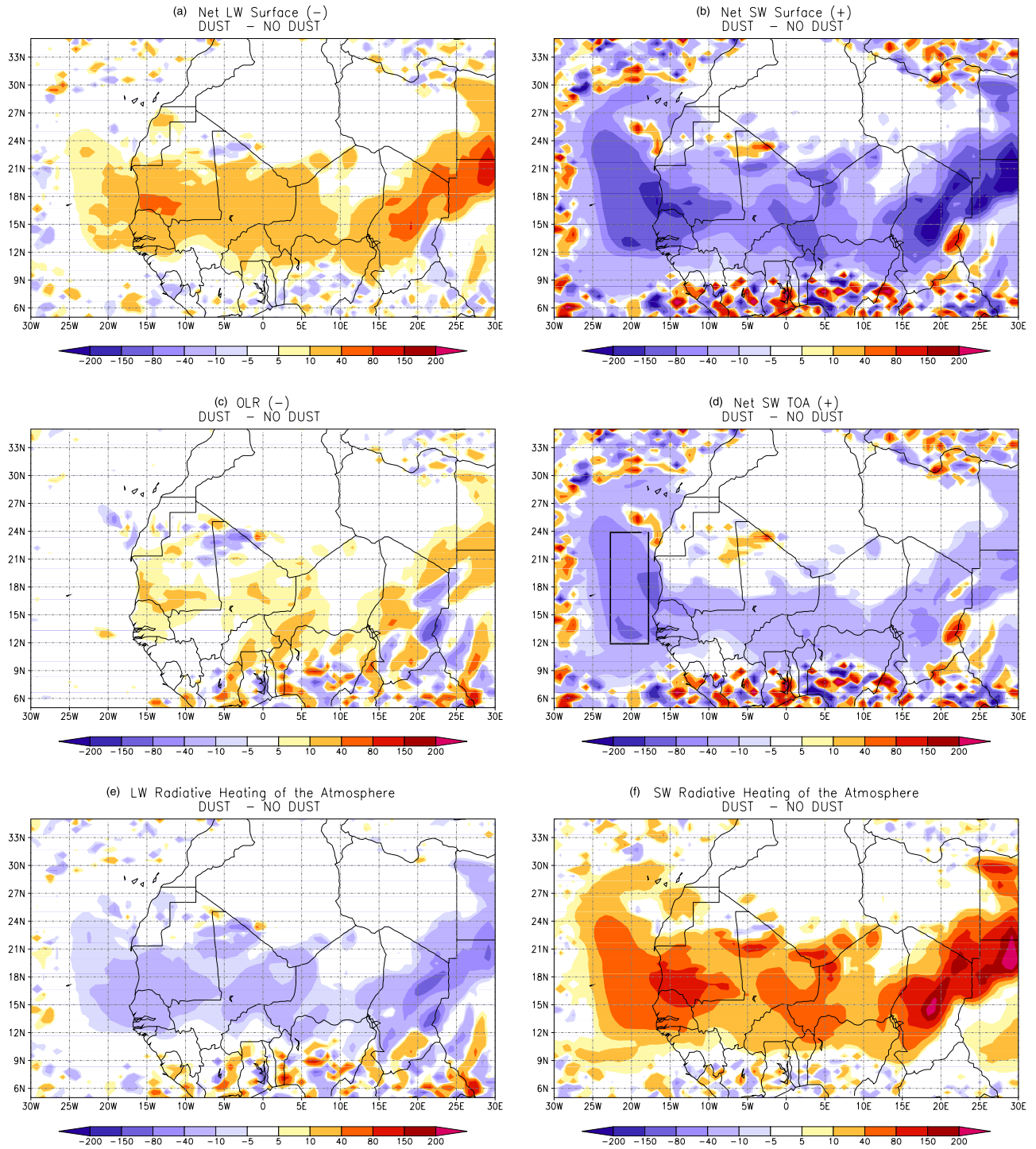


Figure 14. The radiative impact of modeled dust (= DUST – NODUST) on the day 4 forecasts of surface and TOA radiative fluxes from the forecast initialized at 1200 UTC 4 March 2006. (a) Δ LW surface, (b) net SW surface, (c) Δ OLR, and (d) Δ Net SW TOA. (e and f) The Δ LW and Δ SW radiative heating of the atmosphere given by the radiative divergence (TOA – surface). The model dust forecasts use the standard dust set up. The box over the western Atlantic in Figure 14d is used for calculations in Figure 15.

to the absorption of SW radiation. This has a small impact on the large cold bias of over 1°C at these heights. A vertical section at 15°N of DUST-NODUST impacts on temperatures shows a consistent cooling of the lowest 1 km,

warming around 1–1.5 km and regions of warming above this in the free troposphere, large in some regions where the modified radiative forcing due to dust interacts with cloud in the model atmosphere. Screen level temperatures are

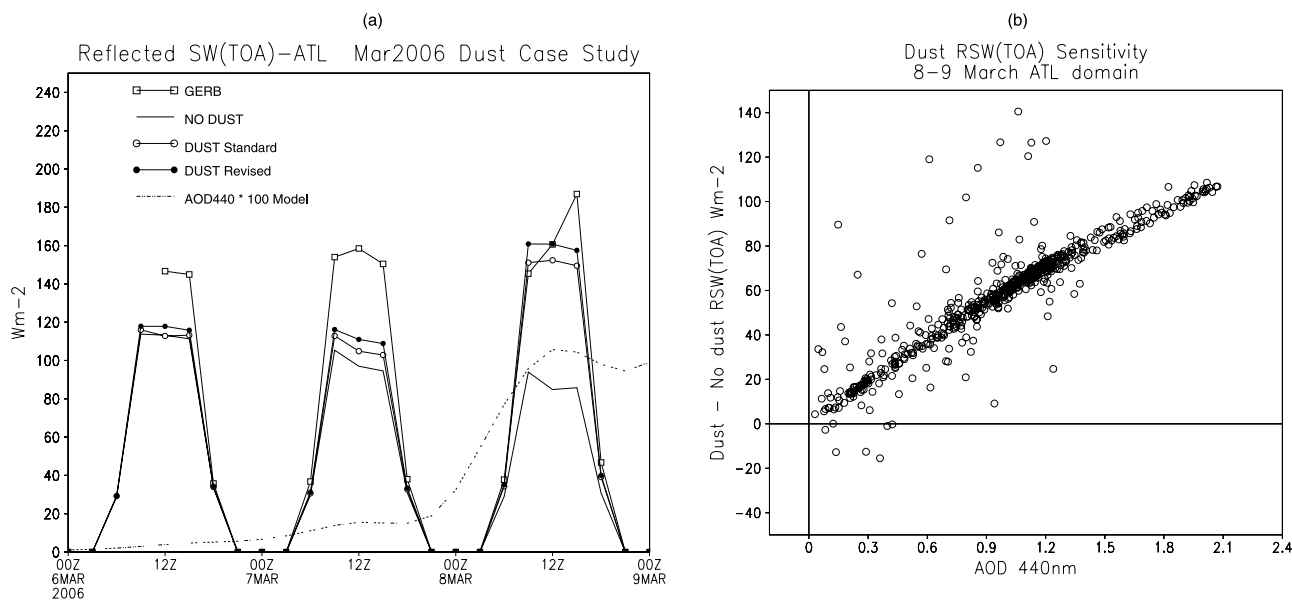


Figure 15. Radiative impacts of dust over the tropical Atlantic domain ($12\text{--}24^{\circ}\text{N}$, $23\text{--}18^{\circ}\text{W}$ (see Figure 14d)). (a) Evolution of reflected SW at TOA for DUST and NODUST forecasts and GERB. The modeled AOD*100 is also shown averaged over this domain. (b) Scatterplot of DUST – NODUST RSW versus model AOD at 440 nm. The model dust forecasts use the standard dust setup (DUST Standard).

suppressed by -0.5 to -1°C over a broad region, with a maximum cooling of over -2°C in Senegal (Figure 16d).

5. Summary and Discussion

[51] In this study we have evaluated the radiative balance of the operational global NWP version of the Met Office Unified Model (MetUM) over West Africa during the 2006 dry season (December–March), using surface observations from the ARM Mobile Facility at Niamey (Niger) available as part of the RADAGAST project and AMMA campaign. Top of the atmosphere fluxes were evaluated against the high spatial and temporal resolution broadband fluxes from GERB. Significant systematic errors were noted in the radiative fluxes at Niamey.

[52] 1. The surface downward SW flux is typically overestimated by around 50 W m^{-2} and on occasions by much larger amounts. Comparison with measurements from the AERONET site at Banizoumbou and further off-line sensitivity tests with the Edwards-Slingo radiation code confirm that the lack of mineral dust and biomass burning aerosols in the model could account for a large proportion of the temporal evolution of errors in the model surface downward SW. Mineral dust and biomass burning aerosols contribute approximately 50% each to the total aerosol optical depth during the December–January period, with the dust contribution increasing steadily in February and reaching 90% during March. This is to be expected because of the seasonal shift in the biomass burning activity.

[53] 2. The reflected SW fluxes are underestimated by the model. Comparisons with the MODIS albedo products point to deficiencies in the specification of current albedo from the *Wilson and Henderson-Sellers* [1985] data set. The Sahel region appears too dark while areas of the Sahara desert and coastal regions around the Red Sea appear too

bright in the model. This has led to operational corrections to model albedo over sparsely vegetated surfaces (model cycle G44, May 2007), with further improvements for vegetated surfaces planned in 2008.

[54] 3. These two errors combine positively to give systematic errors in surface net SW of around $+100\text{ W m}^{-2}$, leading to excessive warming of the surface, an overestimate in sensible heat flux and a daytime warm bias of 3 to 6°C in screen level temperatures.

[55] 4. Errors are smaller for the surface longwave (LW) radiative fluxes, although there were systematic differences linked to the evolution of the diurnal cycle with too much cooling in the late afternoon and during the night and too little at other times of the day. The use of a 3 h radiation time step severely compromises the LW fluxes introducing a systematic 1.5 h lag in the modeled fluxes compared to observations.

[56] 5. Similar errors were noted for the TOA fluxes with the model reflecting too little SW on cloud-free days over Niamey compared to observations from GERB. OLR is too large, particularly on cloud-free days with high aerosol loading (e.g., 8 March). Again this is attributed to the lack of radiative forcing from mineral dust as outlined by *Haywood et al.* [2005].

[57] 6. Preliminary radiative divergence calculations at Niamey (taking no account of surface heterogeneity) showed too little SW heating of the atmospheric column and too much LW cooling. This leads to a net radiative cooling error of around -0.1 K/d over the full diurnal cycle and -0.25 K/d for daytime. This radiative error may have implications for the hydrological cycle with the model atmosphere tending to be more unstable.

[58] To further quantify the role of mineral dust on the forecasts we implemented the dust parametrization of *Woodward* [2001] in the global and regional NWP models

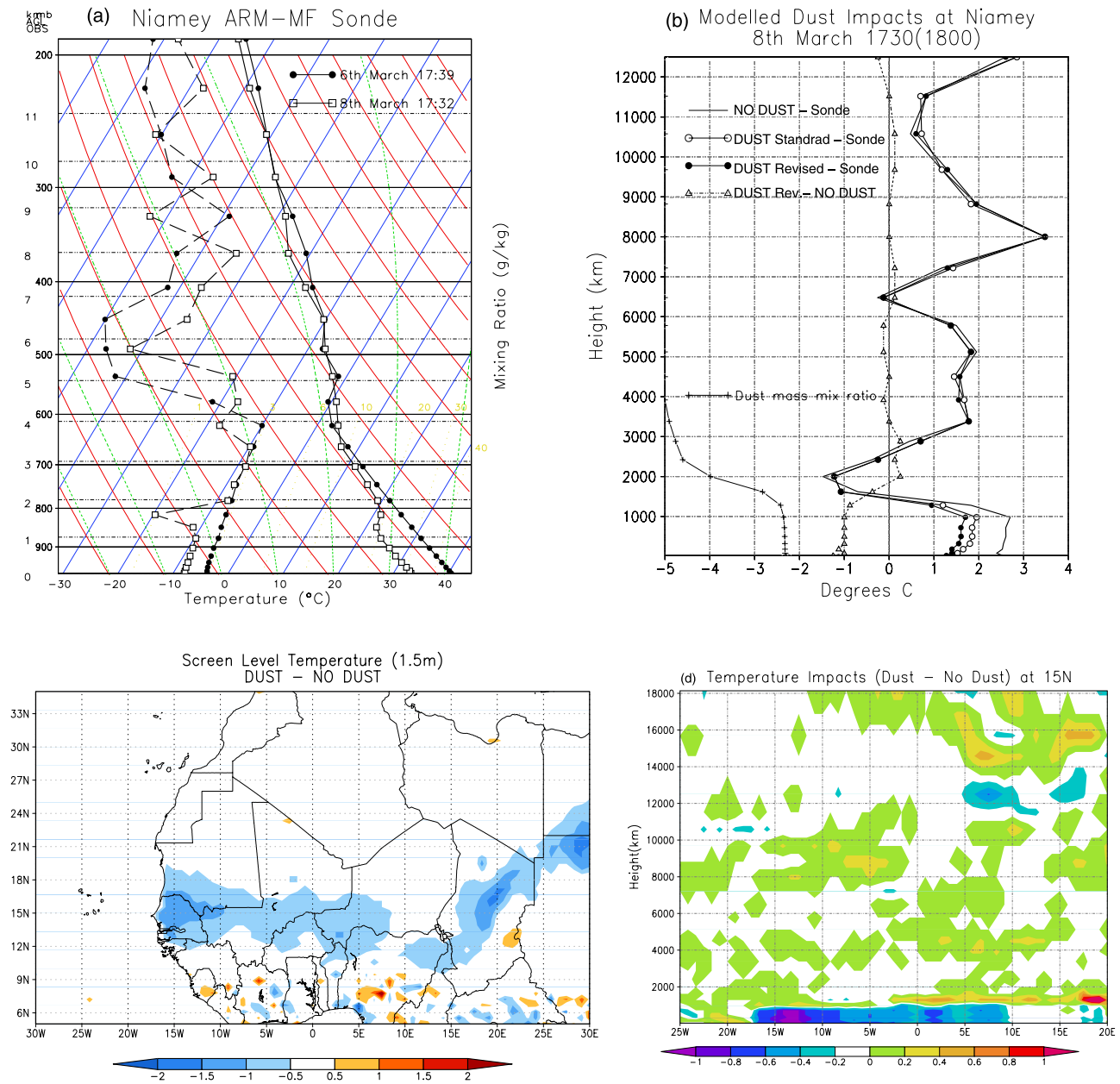


Figure 16. Impacts of mineral dust (DUST – NO DUST) on the vertical thermodynamic structure and screen level temperatures. (a) Skew-T plot of sonde data from 6 and 8 March 2006 (1730h), (b) temperature biases (model – sonde) in UM forecasts with and without dust parameterization (DUST Standard). Also shown in this panel is (1) the DUST – NO DUST difference for the sensitivity experiment (DUST Revised, see text) and (2) the dust mass mixing ratio for dust bin 4, where the max value is $1e-7$ kg/kg. (c) impact of dust (DUST Standard) on screen level temperatures at 1200 UTC 8 March 2006 (day 4 forecast). (d) Vertical section (0–18 km) of dust impacts (DUST Standard) on temperatures along 15°N.

[see *Greed et al.*, 2008]. The major dust outbreak of 6–12 March 2006 has been used to evaluate dust predictions and radiative impacts in the NWP models. This event was strongly forced on large scales from the midlatitudes and the operational global NWP models showed good predictability of the near surface flow over West Africa out to 4–5 days lead time, making this a good case for evaluating the dust parameterization. The model captures the genesis of the dust outbreak in the lee of the Saharan Atlas mountains and advection south over Niamey and west over the tropical

Atlantic, and to some extent the emissions over preferential source regions (e.g., Bodélé) behind the dust front. However, the AOD in the model were underestimated compared to AERONET observations. Possible reasons include (1) errors in the geographical distribution/properties of dust sources from the IGBP soils data sets, (2) uncertainties in the parameterization of dust uplift, (3) errors in the specification of soil moisture, (4) errors in the modeled relationship between soil moisture and dust uplift, (5) potential problems in modeling diurnal variations in near surface

wind important for dust uplift [Todd et al., 2008], (6) no account is currently taken of subgrid-scale gustiness in the wind field which may play a role in dust production for 60 km model grid boxes used here [e.g., Cakmur et al., 2004], or (7) inadequate dust amounts due to initializing dust forecasts with zero dust loadings. More research on these issues is required, including performance at higher horizontal resolutions and sensitivity to soil moisture state.

[59] The modeled dust had largest impacts on the SW radiative fluxes due to scattering and absorption, with an increase in reflected SW at the TOA, particularly large for the bright dust over the dark ocean, and a larger overall decrease in the net SW at the surface. The dust led to a SW heating of the atmospheric column of $>40 \text{ W m}^{-2}$ for AODs > 0.7 . This reduces errors in the SW radiation budget and showed better verification against GERB over the West Africa coast and against ARM-MF and GERB at Niamey. The impacts of dust on LW fluxes were much smaller with reductions in OLR of $5\text{--}40 \text{ W m}^{-2}$ and an increased surface net LW forcing of $10\text{--}80 \text{ W m}^{-2}$. As the surface LW radiative flux impacts were larger than those at the TOA the overall LW impact on the column was to cool by -5 to -40 W m^{-2} , partially offsetting the SW warming. The dust surface forcing was for a radiative cooling dominated by the reduction in downward SW, leading to a cooler surface and screen level temperatures, and alleviating the model's daytime warm bias.

[60] This study has shown that neglect of mineral dust (and biomass burning) aerosols play a key role in determining systematic errors in the model's radiative balance over West Africa during the dry season and impact the evolution of the modeled weather via a poor surface energy balance and warm biases in screen level temperatures. Although some improvements are expected from a planned implementation of new seasonally varying climatologies of biomass burning aerosol and mineral dust in the global NWP model, the real challenge lies in being able to predict the temporal evolution of aerosol throughout the seasonal/annual cycle. Such predictions would have great benefits for aviation, humanitarian and military applications in the region, particularly for predictability lead times of at least 2 days seen in the Saharan CAMM [see Greed et al., 2008] and perhaps on occasions out to 4–5 days as seen in the strongly forced 6–12 March dust event in this study.

[61] **Acknowledgments.** Thanks to Marie Doutriaux-Boucher at the Met Office for providing the OMI AI data, Gary Robinson at ESSC for providing the SEVIRI RGB dust products, Helen Brindley at Imperial College for providing advice on accuracy of GERB fluxes under heavy aerosol loadings over the ocean, and Stephanie Woodward at the Met office Hadley Centre for providing updates on dust parameterization for trialing in NWP and general advice on the scheme. Thanks to PIs at AERONET sites for maintaining and providing data: D. Tanré (M'bour (Dakar), Cape Verde, Banizoumbou, DMN Maine Soroa), P. Goloub (Agoufou, Djougou), J.-L. Rajot (DMN Maine Soroa), Bernadette Chatenet (IER Cinzana), and R. Pinker (Ilorin). Thanks to Caroline Houldcroft at University of Swansea for providing revised albedo ancillary files for the Unified Model based on MODIS. Thanks also to the two reviewers who helped improve this paper.

References

- Ackerman, T., and G. Stokes (2003), The Atmospheric Radiation Measurement Program, *Phys. Today*, *56*, 38–44.
- Allan, R. P., A. Slingo, S. F. Milton, and I. Culverwell (2005), Exploitation of Geostationary Earth Radiation Budget data using simulations from a numerical weather prediction model: Methodology and data validation, *J. Geophys. Res.*, *110*, D14111, doi:10.1029/2004JD005698.
- Allan, R., A. Slingo, S. Milton, and M. Brooks (2007), Evaluation of the Met Office global forecast model using Geostationary Earth Radiation Budget (GERB) data, *Q. J. R. Meteorol. Soc.*, *133*, 1993–2010.
- Barkstrom, B., et al. (1989), The Earth Radiation Budget Experiment (ERBE) archival and April 1985 results, *Bull. Am. Meteorol. Soc.*, *70*, 1254–1262.
- Barnum, B., et al. (2004), Forecasting dust storms using the CARMA-dust model and MM5 weather data, *Environ. Modell. Softw.*, *19*, 129–140.
- Beljaars, A. (2001), Issues in boundary layer parametrization for large scale models, paper presented at ECMWF Seminar on Key Issues in the Parametrization of Subgrid Physical Processes, Eur. Cent. for Med.-Range Weather Forecasts, Reading, U.K.
- Bellouin, N., O. Boucher, J. Haywood, C. Johnson, A. Jones, J. Rae, and S. Woodward (2007), Improved representation of aerosols for HadGEM2, Tech. Note 73, Hadley Cent., Met Off., Exeter, U.K.
- Brindley, H., and J. Russell (2006), Improving GERB scene identification using SEVIRI: Infrared dust detection strategy, *Remote Sens. Environ.*, *104*, 426–446.
- Brown, A., R. Beare, J. Edwards, A. Lock, S. Keogh, S. Milton, and D. Walters (2008), Upgrades to the boundary layer scheme in the Met Office NWP model, *Boundary Layer Meteorol.*, in press.
- Cakmur, R. V., R. L. Miller, and O. Torres (2004), Incorporating the effect of small-scale circulations upon dust emission in an atmospheric general circulation model, *J. Geophys. Res.*, *109*, D07201, doi:10.1029/2003JD004067.
- Chou, C., P. Formenti, M. Maille, P. Auset, G. Helas, S. Osborne, and M. Harrison (2008), Size distribution, shape and composition of mineral dust aerosols collected during the AMMA SOP0/DABEX field campaign in Niger, January 2006, *J. Geophys. Res.*, doi:10.1029/2008JD009897, in press.
- Christopher, S. A., P. Gupta, J. M. Haywood, and G. Greed (2008), Aerosol optical thicknesses over North Africa: 1. Development of a product for model validation using TOMS, MISR and AERONET, *J. Geophys. Res.*, doi:10.1029/2007JD009446, in press.
- Cullen, M. (1993), The Unified Forecast Climate Model, *Meteorol. Mag.*, *122*(1559), 81–94.
- Cusack, S., A. Slingo, J. Edwards, and M. Wild (1998), The radiative impact of a simple aerosol climatology on the Hadley Centre climate model, *Q. J. R. Meteorol. Soc.*, *124*, 2517–2526.
- Davies, T., M. Cullen, A. Malcolm, M. Mawson, A. Staniforth, A. White, and N. Wood (2005), A new dynamical core for the Met Office's global and regional modelling of the atmosphere, *Q. J. R. Meteorol. Soc.*, *608*, 1759–1782.
- Edwards, J. M., and A. Slingo (1996), Studies with a flexible new radiation code. I: Choosing a configuration for a large-scale model, *Q. J. R. Meteorol. Soc.*, *122*(531), 689–719.
- Greed, G., J. Haywood, S. Christopher, P. Gupta, S. Milton, A. Keil, and E. Highwood (2008), Aerosol optical thicknesses over North Africa: 2. Modeling and model validation, *J. Geophys. Res.*, doi:10.1029/2007JD009457, in press.
- Grimi, A., G. Myhre, C. Zender, and I. Isaksen (2005), Model simulations of dust sources and transport in the global atmosphere: Effects of soil erodibility and wind speed variability, *J. Geophys. Res.*, *110*, D02205, doi:10.1029/2004JD005037.
- Grimi, A., P. Tulet, and L. Gomes (2006), Dusty weather forecasts using the MesoNH mesoscale atmospheric model, *J. Geophys. Res.*, *111*, D19205, doi:10.1029/2005JD007007.
- Harries, J., et al. (2005), The Geostationary Earth Radiation Budget (GERB) experiment, *Bull. Am. Meteorol. Soc.*, *86*, 945–960.
- Haywood, J., and O. Boucher (2000), Estimates of the direct and indirect radiative forcing due to tropospheric aerosols: A review, *Rev. Geophys.*, *38*, 513–543.
- Haywood, J. M., R. P. Allan, I. Culverwell, T. Slingo, S. Milton, J. Edwards, and N. Clerbaux (2005), Can desert dust explain the outgoing longwave radiation anomaly over the Sahara during July 2003?, *J. Geophys. Res.*, *110*, D05105, doi:10.1029/2004JD005232.
- Heinold, B., J. Helmer, O. Hellmuth, R. Wolke, A. Ansmann, B. Martcorena, B. Laurent, and I. Tegen (2007), Regional modeling of Saharan dust events using LM-MUSCAT: Model description and case studies, *J. Geophys. Res.*, *112*, D11204, doi:10.1029/2006JD007443.
- Holben, B., et al. (1998), AERONET—A federated instrument network and data archive for aerosol characterization, *Remote Sens. Environ.*, *66*, 1–16.
- Houldcroft, C., W. Grey, M. Barnsley, C. Taylor, S. Los, and P. North (2008), New vegetation albedo parameters and global fields of background albedo derived from MODIS for use in a climate model, *J. Hydrometeorol.*, in press.
- Hsu, N., J. Herman, O. Torres, B. Holben, D. Tanré, T. Eck, A. Smirnov, B. Chatenet, and F. Lavenue (1999), Comparisons of the TOMS aerosol index with Sun photometer aerosol optical thickness: Results and applications, *J. Geophys. Res.*, *104*(D6), 6269–6280, doi:10.1029/1998JD200086.

- Hsu, N., J. Herman, and C. Weaver (2000), Determination of radiative forcing of Saharan dust using combined TOMS and ERBE data, *J. Geophys. Res.*, *105*, 20,649–20,661.
- Iversen, J., and B. White (1982), Saltation threshold on Earth, Mars and Venus, *Sedimentology*, *29*, 111–119.
- Johnson, B., S. R. Osborne, and J. M. Haywood (2008), Aircraft measurements of biomass burning aerosols over West Africa during DABEX, *J. Geophys. Res.*, doi:10.1029/2007JD009451, in press.
- Knippertz, P., and A. Fink (2006), Synoptic and dynamic aspects of an extreme springtime Saharan dust outbreak, *Q. J. R. Meteorol. Soc.*, *132*, 1153–1177.
- Liu, M., D. Westphal, A. Walker, T. Holt, K. Richardson, and S. Miller (2007), COAMPS real-time dust storm forecasting during Operation Iraqi Freedom, *Weather Forecast.*, *22*, 192–206.
- Marticorena, B., G. Bergametti, B. Aumont, Y. Callot, and C. N'Doumé, and M. Legrand (1997), Modeling the atmospheric dust cycle: 2. Simulation of Saharan dust sources, *J. Geophys. Res.*, *102*(D4), 4387–4404.
- Martin, G. M., M. A. Ringer, V. D. Pope, A. Jones, C. Dearden, and T. J. Hinton (2006), The physical properties of the atmosphere in the new Hadley Centre Global Environment Model, HadGEM1. Part I: Model description and global climatology, *J. Clim.*, *19*, 1274–1301.
- Miller, M., and A. Slingo (2007), The Atmospheric Radiation Measurement (ARM) Mobile Facility (AMF) and its first international deployment: Measuring radiative flux divergence in West Africa, *Bull. Am. Meteorol. Soc.*, *88*, 1229–1244.
- Mishchenko, M., L. Travis, R. Kahn, and R. West (1997), Modeling phase functions for dustlike tropospheric aerosols using a shape mixture of randomly oriented polydisperse spheroids, *J. Geophys. Res.*, *102*(D14), 16,831–16,847.
- Moody, E., M. King, S. Platnick, C. Schaaf, and G. Feng (2005), Spatially complete global spectral surface albedos: Value-added datasets derived from Terra MODIS land products, *IEEE Trans. Geosci. Remote Sens.*, *43*, 144–158.
- Nickovic, S., G. Kallos, A. Papadopoulos, and O. Kakaliagou (2001), A model for prediction of desert dust cycle in the atmosphere, *J. Geophys. Res.*, *106*(D16), 18,113–18,129.
- Osborne, S. R., B. Johnson, and J. M. Haywood (2008), Physical and optical properties of mineral dust aerosol during the Dust and Biomass-burning Experiment, *J. Geophys. Res.*, doi:10.1029/2007JD009551, in press.
- Özsoy, E., N. Kubilay, S. Nickovic, and C. Moulin (2001), A hemispheric dust storm affecting the Atlantic and Mediterranean in April 1994: Analyses, modeling, ground-based measurements and satellite observations, *J. Geophys. Res.*, *106*, 18,439–18,460.
- Perez, C., S. Nickovic, G. Pejanovic, J. M. Baldasano, and E. Özsoy (2006), Interactive dust-radiation modeling: A step to improve weather forecasts, *J. Geophys. Res.*, *111*, D16206, doi:10.1029/2005JD006717.
- Phillips, T., et al. (2004), Evaluating parametrizations in general circulation models—Climate prediction meets weather prediction, *Bull. Am. Meteorol. Soc.*, *85*, 1903–1915.
- Prospero, J. M., P. Ginoux, O. Torres, S. E. Nicholson, and T. E. Gill (2002), Environmental characterization of global sources of atmospheric soil dust identified with the NIMBUS 7 Total Ozone Mapping Spectrometer (TOMS) absorbing aerosol product, *Rev. Geophys.*, *40*(1), 1002, doi:10.1029/2000RG000095.
- Rawlins, F., S. Ballard, K. Bovis, A. Clayton, D. Li, G. Inverarity, A. Lorenc, and T. Payne (2007), The Met Office global 4-dimensional variational data assimilation scheme, *Q. J. R. Meteorol. Soc.*, *133*, 347–362.
- Redelsperger, J.-L., C. D. Thorncroft, A. Diedhou, T. Lebel, D. J. Parker, and J. Polcher (2006), African Monsoon Multidisciplinary Analysis: An international research project and field campaign, *Bull. Am. Meteorol. Soc.*, *87*, 1739–1915.
- Schmetz, J., P. Pili, S. Tjemkes, D. Just, J. Kerkmann, S. Rota, and A. Ratier (2002), An introduction to Meteosat Second Generation (MSG), *Bull. Am. Meteorol. Soc.*, *83*, 977–992.
- Settle, J., N. A. Bharmal, G. Robinson, and A. Slingo (2007), A comparison of broad-band fluxes at the main and auxiliary sites during the AMF RADAGAST campaign, paper presented at Seventeenth Atmospheric Radiation Measurement (ARM) Science Team Meeting, U.S. Dep. of Energy, Monterey, Calif. (Available at <http://www.arm.gov/publications/proceedings/conf17/index.php>)
- Slingo, A., et al. (2006), Observations of the impact of a major Saharan dust storm on the atmospheric radiation balance, *Geophys. Res. Lett.*, *33*, L24817, doi:10.1029/2006GL027869.
- Tanré, D., J. Geleyn, and J. Slingo (1984), First results of the introduction of an advanced aerosol-radiation interaction in the ECMWF low resolution global model, in *Aerosols and Their Climatic Effects*, pp. 133–177, A. Deepak, Hampton, Va.
- Tegen, I., M. Hoorig, I. Fung, D. Jacob, and J. Penner (1997), Contribution of different aerosol species to the global aerosol extinction optical thickness: Estimates from model results, *J. Geophys. Res.*, *99*, 23,895–23,915.
- Todd, M., R. Washington, S. Raghavan, G. Lizcano, and P. Knippertz (2008), Regional model simulations of the Bodélé low-level jet of northern Chad during the Bodélé Dust Experiment (BoDEX 2005), *J. Clim.*, in press.
- Tulet, P., M. Mallet, V. Pont, J. Pelon, and A. Boone (2008), The 7–13 March dust storm over West Africa: Generation, transport, and vertical stratification, *J. Geophys. Res.*, doi:10.1029/2008JD009871, in press.
- Uno, I., et al. (2006), Dust model intercomparison (DMIP) study over Asia: Overview, *J. Geophys. Res.*, *111*, D12213, doi:10.1029/2005JD006575.
- Walters, D., M. Willett, and S. Milton (2006), A note on the frequency of radiation calculations in the Unified Model, Forecast. Res. Tech. Rep., 485, Met Off., Exeter, U.K.
- Washington, R., M. Todd, N. Middleton, and A. Goudie (2003), Dust-storm source areas determined by the total ozone monitoring spectrometer and surface observations, *Ann. Assoc. Am. Geogr.*, *93*, 297–313.
- Weaver, C., P. Ginoux, N. Hsu, M.-D. Chou, and J. Joiner (2002), Radiative forcing of Saharan dust: GOCART model simulations compared with ERBE data, *J. Atmos. Sci.*, *59*, 736–747.
- Wielicki, B., B. Barkstrom, E. Harrison, R. Lee III, G. Smith, and J. Cooper (1996), Clouds and the Earth's Radiant Energy System (CERES): An Earth Observing System experiment, *Bull. Am. Meteorol. Soc.*, *77*, 853–868.
- Wild, M. (1999), Discrepancies between model calculated and observed shortwave atmospheric absorption in areas with high aerosol loadings, *J. Geophys. Res.*, *104*, 27,361–27,371.
- Wild, M., C. Long, and A. Ohmura (2006), Evaluation of clear-sky solar fluxes in GCMs participating in AMIP and IPCC-AR4 from a surface perspective, *J. Geophys. Res.*, *111*, D01104, doi:10.1029/2005JD006118.
- Wilson, M. F., and A. Henderson-Sellers (1985), A global archive of land cover and soils data for use in general circulation models, *J. Clim.*, *5*, 119–143.
- Woodward, S. (2001), Modeling the atmospheric life cycle and radiative impact of mineral dust in the Hadley Centre climate model, *J. Geophys. Res.*, *106*(D16), 18,155–18,166.
- Zender, C. S., H. Bian, and D. Newman (2003), Mineral Dust Entrainment and Deposition (DEAD) model: Description and 1990s dust climatology, *J. Geophys. Res.*, *108*(D14), 4416, doi:10.1029/2002JD002775.

R. P. Allan and A. Slingo, Environmental Systems Science Centre, University of Reading, Reading RG6 6AL, UK.

M. E. Brooks, G. Greed, J. Haywood, B. Johnson, and S. F. Milton, Met Office, FitzRoy Road, Exeter EX1 3PB, UK. (sean.milton@metoffice.gov.uk)

W. M. F. Grey, Department of Geography, Swansea University, Swansea SA2 8PP, UK.